PHYSICAL REVIEW D VOLUME 22, NUMBER 3 1 AUGUST 1980

High-transverse-momentum symmetric-particle-pair spectra and correlations

John F. Gunion
University of California, Davis, California 95616

B. Petersson
University of Bielefeld, Faculty of Physics, Postfach 8640, D-4800 Bielefeld 1, Germany

(Received 31 December 1979)

We discuss high-p_T production of particle pairs, comparing the "higher-twist" constituent-interchange-model (CIM) subprocesses to the most "elementary" [quantum chromodynamics (QCD)] subprocesses. All aspects of spectra scaling laws and charge and quantum-number correlations are discussed. Comparison with existing data is given. In general, we find that meson pairs at moderate p_T receive contributions from a mixture of QCD and CIM subprocesses; the strongest evidence for the CIM contributions comes from substantial charge correlations observed in several experiments. For pairs involving baryons, especially $p\bar{p}$, CIM should be dominant at moderate p_T with consequent large correlations and strong inverse-p_T damping.

I. INTRODUCTION

Considerable attention has been focused on the production of hadrons at high transverse momentum (p_T) as a probe of the important short-distance subprocesses of quantum chromodynamics (QCD). All theorists agree that the most elementary processes—$qq \to qq$, $qg \to qg$, and $gg \to gg$—with basic p_T^{-4} behavior will dominate at sufficiently large p_T. At moderate p_T in single-particle spectra, however, there are two competing approaches: (1) the constituent-interchange model[1] (CIM) in which higher-twist QCD subprocesses, such as $qM \to qM$, yield intrinsic p_T^{-8} behavior (for meson production) with large normalization that temporarily dominates the more elementary p_T^{-4} subprocesses (QCD subprocesses); and (2) the transverse-fluctuation approach[2] in which the basic p_T^{-4} behavior of the elementary QCD processes is obscured not only by scale breaking, but also by large primordial transverse-momentum fluctuations, of the colliding quarks and gluons within the incoming hadrons, in such a way as to yield temporary p_T^{-8} behavior for single-particle spectra.

The advocates of the CIM note that processes involving bound states are inevitably present in QCD, that their normalization is calculable, and that the predicted moderate-p_T single-particle inclusive spectra are in excellent agreement with data—for instance, the differing behaviors, p_T^{-8} for meson triggers and p_T^{-12} for baryon triggers, are automatic in the CIM while difficult to reconcile in the fluctuation approach. Further, CIM advocates claim that a proper inclusion of off-shell effects[3] greatly reduces the effects of primordial transverse fluctuations and keeps elementary p_T^{-4} subprocesses from being the dominant contribution to single-particle spectra in the moderate-p_T range.

The correlations between two hadrons, H_1 and H_2, produced on opposite sides of the beam axis, especially near the symmetric point $p_{T_1} \sim p_{T_2}$, are a particularly sensitive way to discriminate between these two different types of contributions. The CIM processes, for instance, yield substantial quantum-number correlations between H_1 and H_2 while the elementary QCD processes do not. The two approaches are also distinguishable by the scaling laws of the pair cross section. Near the symmetric point the scaling laws in $p_T = \frac{1}{2}(p_{T_1} + p_{T_2})$ are basically insensitive to the primordial transverse-momentum ("k_T") fluctuations.[4]

In single-particle production a possible configuration (at moderate p_T) is one in which each of the colliding quarks (or gluons) has large intrinsic k_T in the same direction as the trigger p_T [Fig. 1(a)]. This configuration, which probes the subprocess at small (instead of large) momentum transfer is potentially capable of distorting the p_T spectrum, whereas in the absence of k_T fluctuations the subprocess is always evaluated at large momentum transfers. In contrast, for symmetric-pair production, Fig. 1(b), the preferred reaction configuration is initiated by quarks (or gluons) with small k_T. Any bias in the direction of one hadron makes the production of the second, symmetric hadron much less probable. This intuition is confirmed by explicit calculation.[4] Thus in symmetric pair production a comparison of CIM subprocess scaling laws with those of the more elementary p_T^{-4} subprocesses is much less sensitive to k_T fluctuations.

In the present paper, we will calculate the CIM contributions to symmetric-pair production for a variety of quantum-number combinations of the pairs. We also include the elementary QCD contributions without scale breaking. It has been

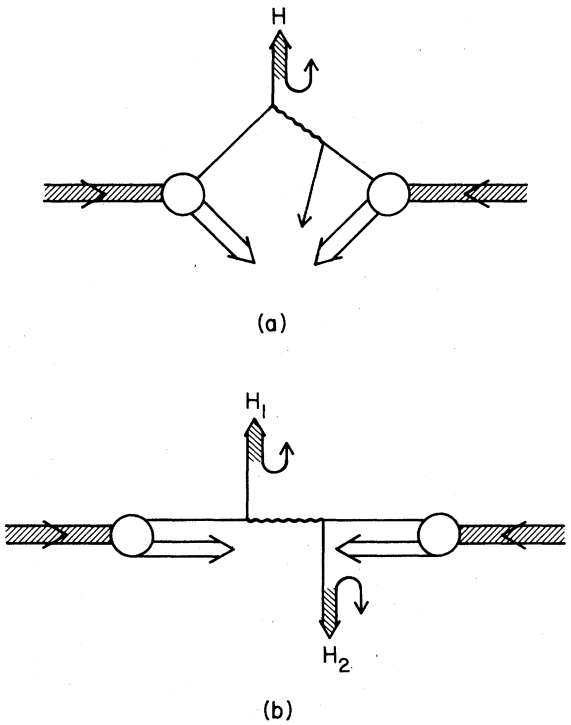

FIG. 1. The contribution configurations for (a) single-particle high-p_T production, and (b) symmetric high-p_T pair production.

shown[5] that this gives a good description of the single-particle spectra in pp collisions at both Fermilab and CERN ISR energies. We use the same relative weight for the two contributions as was used in Ref. 5. We will discover that the predicted pair spectra agree with existing Fermilab data[6] in shape and normalization. The underlying scaling laws are quite different from those predicted on the basis of p_T^{-4} subprocesses only. However, scale-breaking effects in the p_T^{-4} processes tend to make the differences smaller.[2,4] Thus definitive tests of the scaling laws, which are, as we emphasize, free of k_T fluctuation ambiguities, must await corresponding ISR data at widely separated energies.

We *will* see, however, that existing ISR and Fermilab data[7,8] already provide evidence for the quantum-number correlations expected when a mixture of CIM and QCD subprocesses is employed; the large quantum-number correlations are a direct consequence of the structure of the CIM contributions.

In Sec. II we will survey the scaling-law differences for pair spectra, predicted in an asymptotic expansion of the pair cross section, between CIM and QCD p_T^{-4} type subprocesses.

Section III will discuss in greater detail the contributing reactions and contrast CIM and QCD subprocesses. We will compare analytic-asymptotic-expansion techniques with more precise results obtained by numerical integration and discuss general systematics, charge correlations, and related questions. The numerically integrated cross sections have scaling laws that, at experimental moderate-p_T values, differ slightly from those obtained asymptotically. The numerical results yield excellent agreement with the data in shape and normalization. The distinguishing differences between the CIM and p_T^{-4} scaling laws are still apparent. The relative normalization of these two types of contributions is discussed.

Section IV contains concluding remarks and discussion.

The Appendix provides details of the derivations of the asymptotic forms discussed in Sec. II.

We encourage the reader of the paper to lay greatest emphasis on the general features of the higher-twist CIM subprocesses which distinguish them from QCD subprocesses. These features include the scaling laws, charge correlations, and relative cross-section magnitudes. This is especially important since their exact normalization is less trustworthy—the general features can be used to ascertain whether or not the CIM subprocesses are present. The level predicted by the normalization process of Ref. 1 on the basis of a smooth connection to elastic scattering ($pp \to pp$ and $\pi p \to \pi p$) is fairly substantial. Doubt, however, has been cast on this normalization procedure in the case of π beams by the data of Frisch *et al.*[9] who find the ratio $(\pi^- p \to \pi^- X)/(\pi^- p \to \pi^+ X)$ to be very near 1 at high p_T for a variety of x_F values. This is in contradiction to the extension of Ref. 5 to CIM subprocesses contributions for pion beams; a much larger ratio is obtained. However, QCD subprocesses also have difficulty at the higher x_F values of the above data; they predict π^-/π^+ approximately 3 times larger than the data.[10] Thus the failure of the final π^- to remember that it comes from a π^- beam is not fully understood in either model. Various excuses can be proposed in either approach but it is apparent that a clear means of discriminating them in the case of pp collisions is highly desirable. This paper emphasizes that high-p_T pair correlations and scaling laws provide just such a means. Especially important are the scaling laws and cross-section ratios for $pp \to ppX$, $pp \to p\bar{p}X$, and $pp \to p\pi X$ which are *very* different from those predicted by QCD. The single-particle predictions of the higher-twist CIM subprocesses for $pp \to pX$ and $pp \to \bar{p}X$ have long been one of the model's particular successes—those reactions not being well described by the simpler QCD subprocesses.

II. COMPARISON OF ASYMPTOTIC SCALING LAWS

We will be concerned with three distinct final-state structures in our calculations. These are illustrated in Figs. 2(a)–2(c). They differ according to the number of final-state fragmentations required. We consider the reaction $A+B\to C+D+X$. The high transverse momenta of C and D are produced through a large-angle subprocess scattering of secondaries a and b of A and B, respectively. In the first situation, Fig. 2(a), C and D are produced directly in the subprocess via $a+b\to C+D$. In the second situation, Fig. 2(b), final fragmentation occurs, $a+b\to C+d$ at large angle followed by $d\to D$ fragmentation. In the third structure, Fig. 2(c), both C and D are produced indirectly, $a+b\to c+d$ at large angle followed by $d\to D$ and $c\to C$. In all three cases mentioned above the pair cross section can be derived from the formula

$$E_C E_D \frac{d\sigma}{d^3p_C d^3p_D} = \frac{s}{2\pi}\int dx_a dx_b d^2k_a d^2k_b dw_c dw_d d^2k_c d^2k_d x_a G_{a/A}(x_a,\bar{k}_a) x_b G_{b/B}(x_b,\bar{k}_b) \times \frac{D_{C/c}(w_c,\bar{k}_c)}{w_c^2}\frac{D_{D/d}(w_d,\bar{k}_d)}{w_d^2}\frac{d\sigma^{ab\to cd}}{d\hat{t}}\delta^4(p_a+p_b-p_c-p_d)\,. \tag{2.1}$$

In the case of direct production of, e.g., particle C, one should replace $D_{C/c}(w_c,\bar{k}_c)$ by $\delta(w_c-1)\delta^2(\bar{k}_c)$. The variables w_i and k_i, $i=a,b,c,d$ are respectively, the scaled longitudinal and the internal transverse fluctuation momenta.

In contrast to calculations for single-particle spectra, the pair spectra will be insensitive to the way in which we incorporate the internal ("primordial") transverse momenta k_i. The only critical feature is that the behavior in the k_i be more rapidly damped than a power law. All power laws are contained in the various possible short-distance subprocess cross sections.

We employ a Gaussian form for the primordial transverse k_T fluctuations:

$$G_{a/A}(x_a,\bar{k}_a) = G_{a/A}(x_a)\frac{a}{\pi}e^{-ak_a^2}, \tag{2.2}$$

$$D_{C/c}(w_c,\bar{k}_c) = D_{C/c}(w_c)\frac{c}{\pi}e^{-ck_c^2}. \tag{2.3}$$

In practice we choose

$$\frac{1}{a}=\frac{1}{b}=\langle k^2\rangle, \tag{2.4}$$

$$\frac{1}{c}=\frac{1}{d}=\langle l^2\rangle. \tag{2.5}$$

Furthermore, we use the simple parametrizations of Ref. 5, which led to a successful description of single-particle spectra. Typically they are of the form

$$x_a G_{a/A}(x_a) = \Lambda_{a/A}(1-x_a)^{g_{a/A}}, \tag{2.6}$$

$$D_{D/d}(w_d) = d_{D/d}\frac{(1-w_d)^{g_{D/d}}}{w_d}. \tag{2.7}$$

We will only need the cross sections at 90°,

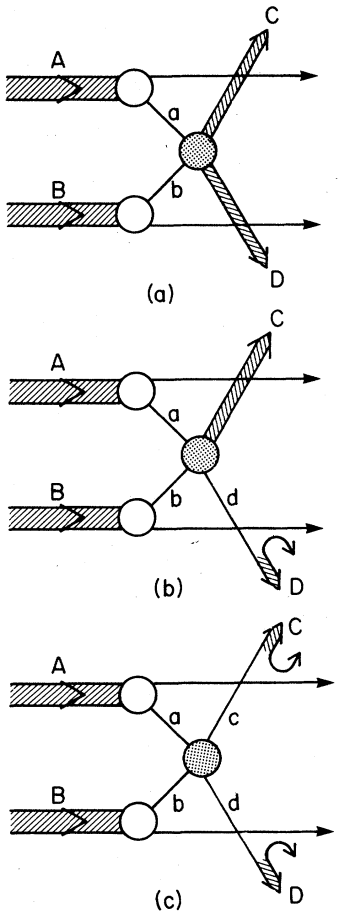

FIG. 2. Production of a back-to-back pair of high-p_T particles: (a) when both are produced directly by the subprocess, (b) when one is obtained as a fragment of a primary particle produced directly by the subprocess while the other is produced directly, and (c) when both are produced as secondary fragments of primary particles produced directly by the subprocess.

where they can be written in the form

$$\frac{d\sigma}{d\hat{t}} = \frac{\pi \mathfrak{D}_{90^\circ}}{\hat{s}^N} . \tag{2.8}$$

The parameters $\Lambda_{a/A}$, $g_{a/A}$, $d_{D/d}$, $g_{D/d}$, and $\mathfrak{D}^{90^\circ}$ are given for all processes of interest in Ref. 5. We will not discuss their determination here. From the formulas given above we may now infer the asymptotic scaling limits for the three cases of interest. We refer to the Appendix for the explicit derivations.

We are interested in the situation where particles C and D are produced opposite to each other at 90°:

$$\vec{p}_{T_D} = -z\vec{p}_{T_C} . \tag{2.9}$$

For simplicity we discuss in the text mainly the case $z \approx 1$ (the symmetric point).[11]

In the first situation, the direct production of particles C and D [Fig. 2(a)], we obtain at the symmetric point

$$E_C E_D \frac{d\sigma}{d^3p_C d^3p_D} \simeq \frac{1}{2\pi\langle k^2\rangle} \Lambda_{a/A}\Lambda_{b/B} \mathfrak{D}_{90^\circ}^{ab\to CD} \times \frac{(1-x_T)^{g_{a/A}+g_{b/B}}}{(2p_T)^{2N}} . \tag{2.10a}$$

Away from the symmetric point the cross section vanishes exponentially; for $p_{T_C} - p_{T_D} = \Delta p_T$ fixed we get

$$E_C E_D \frac{d\sigma}{d^3p_C d^3p_D} = E_C E_D \frac{d\sigma}{d^3p_C d^3p_D}\bigg|_{\text{sym}} \times \exp\left(-\frac{(\Delta p_T)^2}{2\langle k^2\rangle}\right) . \tag{2.10b}$$

Note that the double-differential cross section has the same scaling (p_T^{-2N}) at fixed x_T as the single-particle spectrum $Ed\sigma/d^3p$ for the same subprocess. The extra inverse-momentum dimensions are provided by a transverse-fluctuation scale. This is typical of all the symmetric-pair results; while the scaling laws are simply related to those of the subprocess, the overall normalization requires knowledge of the size of the transverse fluctuations. The sensitivity arises simply from the momentum balance constraints transverse to the incoming beam direction.

The most important configuration for the CIM contributions is that illustrated in Fig. 2(b),[11] with one final fragmentation. Here we consider two different limits, $z = 1$ and $z < 1$.

We find

$$E_C E_D \frac{d\sigma}{d^3p_C d^3p_D} = \frac{1}{2\pi\langle k^2\rangle} \Lambda_{a/A}\Lambda_{b/B} \left(\frac{2\langle k^2\rangle}{2\langle k^2\rangle + 2\langle l^2\rangle}\right)^{1/2} \mathfrak{D}_{90^\circ}^{ab\to Cd} \frac{(1-x_T)^{g_{a/A}+g_{b/B}}}{(2p_T)^{2N}} I(z, p_T) . \tag{2.11}$$

For $z < 1$,

$$I(z, p_T) \xrightarrow[p_T \text{ large}]{} \frac{1}{z} D_{D/d}(z)\sqrt{\pi} \frac{(2\langle k^2\rangle)^{1/2}}{p_T} , \tag{2.12}$$

and for $z = 1$,

$$I(1, p_T) \xrightarrow[p_T \text{ large}]{} d_{D/d} \left(\frac{(2\langle k^2\rangle)^{1/2}}{p_T}\right)^{g_{D/d}+1} \int_0^\infty \alpha^{g_{D/d}} e^{-\alpha^2} d\alpha . \tag{2.13}$$

Clearly, as $z \to 1$ a rough interpolation is provided by the replacement

$$(1-z) \to \frac{(\langle k^2\rangle)^{1/2}}{p_T} . \tag{2.14}$$

Thus the scaling laws are quite different in the two regimes $p_T^D \simeq p_T^C = p_T$ and $p_T^D = zp_T^C = zp_T$. In the case of approximate equality, transverse-momentum constraints impose additional inverse powers of p_T through the fragmentation functions.

Finally we consider the double-fragmentation case, Fig. 2(c). Here we obtain in the symmetric case

$$E_C E_D \frac{d\sigma}{d^3p_C d^3p_D} = \frac{1}{[2\pi(\langle k^2\rangle + \langle l^2\rangle)]^{1/2}} \frac{1}{p_T} \Lambda_{a/A}\Lambda_{b/B} d_{D/d} d_{C/c} \mathfrak{D}_{90^\circ}^{ab\to cd} \frac{(1-x_T)^{g_{a/A}+g_{b/B}+g_{C/c}+g_{D/d}}}{(2p_T)^N} \times \frac{\Gamma(g_{a/A}+g_{b/B}+1)\Gamma(g_{C/c}+g_{D/d}+1)}{\Gamma(g_{a/A}+g_{b/B}+g_{C/c}+g_{D/d}+2)} J(x_T) , \tag{2.15}$$

where

$$J(x_T) \xrightarrow[x_T \to 1]{} 1 .$$

J is specified in detail in the Appendix.

Note that in the double-fragmentation situation, the symmetric-pair cross section scales with one more power than the single-particle cross section based on the same subprocesses.

Let us now discuss the implications of (2.10),

(2.11), and (2.15) for two typical subprocesses—a higher-twist, CIM subprocess, quark + meson → quark + meson, and a p_T^{-4} subprocess, $qq \to qq$. We will consider proton-proton collisions with production of an exactly symmetric pair of π mesons (i.e., $z = 1$). In the CIM case $qM \to qM'$, one of the observed mesons must be the fragment of the final quark; the other observed meson can be produced directly in the subprocess or indirectly as the decay product of a meson resonance. For $qq \to qq$ we obtain both mesons via quark fragmentation. In summary we consider

$$qq \to q \quad q \quad , \qquad \text{(2.16a)}$$
$$\qquad\quad \searrow \pi_1 \quad \searrow \pi_2$$

$$qM' \to \pi_1 \quad q \quad , \qquad \text{(2.16b)}$$
$$\qquad\qquad\quad \searrow \pi_2$$

$$qM' \to M^* \quad q \quad , \qquad \text{(2.16c)}$$
$$\qquad\qquad\quad \searrow \pi_1 \quad \searrow \pi_2$$

where we presume $M^* = \rho$ is typical. The required scaling-law parameters are

$$\frac{d\sigma^{qM' \to M^* q}}{d\hat{t}} \propto 1/\hat{s}^4 ,$$

$$\frac{d\sigma^{qq \to qq}}{d\hat{t}} \propto 1/\hat{s}^2 ,$$

$$g_{M/q} = 1 , \qquad \text{(2.17)}$$
$$g_{q/p} = 3 ,$$
$$g_{M/p} = 5 ,$$
$$g_{\pi/\rho} = 0 .$$

We first remind the reader what the implications of (2.17) are for single-particle production. The scaling laws based on the subprocesses of (2.16) are

$$E_{\pi_1} \frac{d\sigma}{d^3 p_{\pi_1}} \propto \begin{cases} (1 - x_T)^9 / p_T^{\,4} , & \text{(2.18a)} \\ (1 - x_T)^9 / p_T^{\,8} , & \text{(2.18b)} \\ (1 - x_T)^{10} / p_T^{\,8} . & \text{(2.18c)} \end{cases}$$

We have, of course, temporarily ignored scale violations and primordial transverse-fluctuation effects upon the scaling laws. The phenomenological debate centers on the possibility that combining scale violation and (on-shell) fluctuations tends to make the p_T^{-4} scaling law of (2.18a) quite similar at moderate p_T to the p_T^{-8} scaling law of the $qM \to qM$ subprocess predictions. However, if we follow the CIM advocates and use off-shell kinematics[3] for the primordial fluctuations, they become unimportant leaving only the scale violations; these effectively change[2] the p_T^{-4} of (2.18a) to approximately p_T^{-6}. The scale-violation effects upon the quark-meson-subprocess predictions are much smaller since the subprocess is initiated by a meson; the distribution $G_{M/p}(x)$ is not strongly affected by QCD corrections due to the color-singlet nature of the meson. Also, final-fragmentation scale violation is present in the $qq \to qq$ case through $D_{M/q}$, but not in the CIM case where the π_1 meson is produced directly or through standard resonance decay.

We now compare the pair spectra. For (2.16) we obtain (neglecting scale violation) the scaling laws

$$E_{\pi_1} E_{\pi_2} \frac{d\sigma}{d^3 p_{\pi_1} d^3 p_{\pi_2}} \propto \begin{cases} \dfrac{(1 - x_T)^8}{(\langle k^2 \rangle)^{1/2} p_T^{\,5}} , & \text{(2.19a)} \\ \dfrac{(1 - x_T)^8}{p_T^{\,10}} , & \text{(2.19b)} \\ \dfrac{(1 - x_T)^9}{(\langle k^2 \rangle + \langle l^2 \rangle)^{1/2} p_T^{\,9}} . & \text{(2.19c)} \end{cases}$$

For the CIM subprocesses the single-fragmentation power law, p_T^{-10}, is higher than that for double fragmentation, p_T^{-9}, but has a large coefficient and will generally tend to dominate at moderate p_T.

Again there is a difference of at least four powers in p_T between the $qq \to qq$ subprocess scaling law and that based on $qM \to qM$. Scale violations will again affect (2.19b) and (2.19c) much less than they will affect (2.19a) where calculations have shown[4] that scale breaking alters the p_T^{-5} to approximately p_T^{-8}. As in the single-particle spectra, one is left with a difference of about $p_T^{\,2}$ between the CIM and p_T^{-4} scaling laws. The advantage of the pair-production configuration is that primordial transverse fluctuations will not further reduce this difference, regardless of how they are incorporated. In addition we shall demonstrate in the next section that the CIM subprocesses produce very substantial charge and quantum-number correlations. These are absent when the symmetric pairs are presumed to be produced by the elementary QCD subprocesses.

III. DETAILED RESULTS

In this section we present numerical results for a variety of pair cross sections. Since the asymptotic scaling laws (2.12), (2.13), and (2.15) are not fully realized at the moderate-p_T values of interest we will give results obtained by exact numerical integration of the functions $I(z, p_T)$ and $J(x_T)$. As an aid in considering the nature and relative size of the contributions from different subprocesses we also tabulate analytic forms and corresponding results (at $z = 1$) based on analytic ap-

proximations (derived in the Appendix), $\bar{I}(1, p_T)$ and $\bar{J}(x_T)$, related to $I(1, p_T)$ and $J(x_T)$. Both $\bar{I}$ and $\bar{J}$ are defined so that as $p_T \to \infty$ or $x_T \to 1$, respectively, they approach unity. For instance, when $x_T > 0.6$, $\bar{J} = J$, where J is the exact function, within 20%. $\bar{I}$ is generally a very reliable approximation while $\bar{J}$ is typically, for $x_T \simeq 0.3$, smaller by a factor of ~2 than J.

In the following tables we present results for exactly symmetric pairs ($z = 1$). We consider first CIM contributions. The tables in the CIM case give for each subprocess (1) an asymptotic analytic expression multiplied by the appropriate $\bar{I}$ correction integral, (2) the numerical results at $x_T = 0.25$, $p_T = 3$ GeV following from exact integration of I, and (3) the result at this same kinematic point following from the $\bar{I}$ approximation. The QCD tables give for each subprocess (1) the analytic result from (2.15) with $J \to \bar{J}$, which is accurate numerically for $x_T > 0.6$, (2) the numerical evaluation at $x_T = 0.25$, $p_T = 3$ GeV of the analytic result, and (3) the result of an exact integration of $J(x_T)$ at the same kinematic point. All results in the tables will be for p-N collisions with cross sections quoted in GeV units and "per nucleon."

We will use these results, in particular, to discuss pair-spectra ratios, such as $pN \to \pi^+\pi^-/\pi^+K^-/\pi^-K^+/K^-K^+$. These ratios depend mostly on relative normalizations of the distribution functions and subprocess cross sections which enter. They provide a useful characterization of many of the overall features of the pair-spectra predictions.

The distribution function and subprocess normalizations we employ, i.e., the $\Lambda_{i/I}$'s, $d_{J/j}$'s, $g_{i/I}$'s, $\mathfrak{D}_{90^\circ}^{ab\to cd}$'s, etc., were given in Ref. 5 where single-particle spectra were predicted. In that reference, however, SU(3) symmetry was used as a working approximation. Here we wish to allow for possible SU(3) breaking through the following additional parameters.

First, for the momentum fractions of Ref. 5 [recall that $\Lambda_{i/I} = f_{i/I}(1 + g_{i/I})$ where $f_{i/I}$ is the fraction of momentum which i carries in I] we define the following:

(a) $f_{s/p} = f_{\bar{s}/p} = \gamma f_{\bar{u}\text{ or }\bar{d}/p}$ and $f_{\bar{u}/p}$ is taken to equal $f_{\bar{q}/p}$ of Ref. 5;

(b) $f_{M(d\bar{s})/p} = \alpha f_{M(d\bar{u})/p}$ and $f_{M(s\bar{s})/p} = \alpha' f_{2\bar{q}/p}$, where $f_{M(d\bar{u})/p}$ and $f_{2\bar{q}/p}$ are taken from Ref. 5;

(c) $d_{K^+/u} = \delta d_{\pi^+/u}$, $d_{K^+,K^-/s} = \delta' d_{\pi^+,\pi^-/s}$, and $d_{K^+/\bar{s}} = d_{K^-/s} = d_{\pi^+/u}$, where $d_{\pi^+/u,s}$ is taken from Ref. 5.

For the subprocess parameters we define the following:

(d) $\alpha_M[M(\bar{s}^u_{\bar{d}}) \to \bar{s} + {}^u_d)] = \sqrt{\kappa}\,\alpha_M[M(\bar{d}u) \to \bar{d} + u]$ and $\alpha_M[M(\bar{s}s) \to \bar{s} + s] = \sqrt{\kappa'}\,\alpha_M[M(\bar{d}u) \to \bar{d} + u]$, where $(4\pi\alpha_M)^{1/2}$ is the vertex describing the breakup of a meson into its quark and antiquark components. The size of $\mathfrak{D}_{90^\circ}^{q_1^M 1 \to q_2 M_2}$ is determined by $\alpha_{M_1}\alpha_{M_2}$ so that, for instance,

$$\left.\begin{matrix} \mathfrak{D}_{90^\circ}^{u\bar{K}^+\to uK^+} \\ \mathfrak{D}_{90^\circ}^{s\pi^0\to uK^-} \\ \mathfrak{D}_{90^\circ}^{u\phi\to sK^+} \\ \mathfrak{D}_{90^\circ}^{s\phi\to s\phi} \end{matrix}\right\} = \mathfrak{D}_{90^\circ}^{u\pi^+\to u\pi^+} \begin{cases} \kappa\,, \\ \sqrt{\kappa}\,, \\ \sqrt{\kappa}\,\sqrt{\kappa'}\,, \\ \kappa'\,. \end{cases} \tag{3.1}$$

We will, in what follows, take $\kappa = \kappa'$. In the above $\mathfrak{D}_{90^\circ}^{u\pi^+\to u\pi^+}$ is proportional to $\alpha_M{}^2$ ($\simeq 4$ GeV^4) as defined in Refs. 1 and 5.

We will take $\langle k^2\rangle = \langle l^2\rangle = 0.5$ GeV^2 for all results that follow. We also define $f_{d/p} = rf_{u/p}$ from Ref. 5.

We begin with a discussion of the various meson-particle-pair ratios for pN collisions. We first summarize the various subprocess configurations which contribute to each type of meson pair in Table I; Table II presents the asymptotic forms and appropriate $\bar{I}$ correction factors. Subprocess contributions which are small in absolute magnitude are not given. For instance, the (st) topologies for the $qM \to qM$ scattering subprocesses are negligible except for K^-K^+ pairs; they are suppressed because of their topology by a factor of 16 relative to the (ut) topologies. Special note should be made of the fusion contributions to K^+K^- and $\pi^+\pi^-$ production.

In Table II we have evaluated the relative magnitudes of the various meson-pair cross sections at the typical point $p_T = 3$ GeV, $x_T = 2p_T/\sqrt{s} = 0.25$, taking all SU(3)-breaking parameters to be $\frac{1}{2}$, and $r = \frac{1}{2}$. The ordering of cross sections is seen to be

$$\pi^+\pi^- > \pi^+\pi^+ > \pi^-\pi^- > K^+\pi^- \gtrsim K^+\pi^+ > K^+K^- > K^+K^+ > \pi^+K^- > K^-\pi^- > K^-K^-\,. \tag{3.2}$$

The relative size of the fusion contribution to the K^+K^- and $\pi^+\pi^-$ cross sections is sensitive to the $\langle k^2\rangle$ value chosen, varying as $1/\langle k^2\rangle$. We employ $\langle k^2\rangle = 0.5$ GeV^2. If $\langle k^2\rangle$ is larger then K^+K^- approaches $K^+K^+(\simeq \pi^+K^-)$.

Cross sections for symmetric $\pi^+\pi^-$, π^+K^-, π^-K^+ and K^+K^- pairs have been obtained by the Stony Brook–Columbia–Fermilab collaboration of Jöstlein *et al.*[6] These are measurements on nuclei and are corrected substantially for A dependence. Near the kinematic point ($p_T = 3$, $x_T = 0.25$) under consideration the cross-section ratios are

$$[\pi^+\pi^- : \pi^-K^+ : K^-\pi^+ : K^+K^-]_{\text{experiment}} = 1.07 : 0.445 : 0.175 : 0.075\,. \tag{3.3}$$

Without A correction the relative size of the K^+K^-

TABLE I. CIM subprocesses. "π^+" indicates *any* meson with quark content the same as a π^+, etc., except where indicated by (*st*) all $q_1M_1 \to q_2M_2$ processes have (*ut*) topology.

Observed pair	Significant subprocesses	SU(3)-breaking factor
$\pi^+\pi^-$	u"π^0" $\to \pi^+ d(\to \pi^-)$	1
	d"π^0" $\to \pi^- u(\to \pi^+)$	1
	$u\bar{u} \xrightarrow{\text{fusion}} \pi^+\pi^-$ + $d\bar{d} \xrightarrow{\text{fusion}} \pi^-\pi^+$	1
$\pi^+\pi^+$	u"π^+" $\to \pi^+ u(\to \pi^+)$	1
$\pi^-\pi^-$	d"π^-" $\to \pi^- d(\to \pi^-)$	1
$K^+\pi^-$	u"K^0" $\to K^+ d(\to \pi^-)$	$\alpha\kappa$
	d"π^0" $\to \pi^- u(\to K^+)$	δ
$K^+\pi^+$	u"π^+" $\to \pi^+ u(\to K^+)$	δ
	u"K^+" $\to K^+ u(\to \pi^+)$	$\alpha\kappa$
K^+K^+	u"K^+" $\to K^+ u(\to K^+)$	$\alpha\kappa\delta$
K^+K^-	u"ϕ" $\to K^+ s(\to K^-)$	$\alpha'\kappa$
	u"π^0" $\xrightarrow{(st)} K^+ s(\to K^-)$	$\sqrt{\kappa}$
	d"π^+" $\xrightarrow{(st)} K^+ s(\to K^-)$	$\sqrt{\kappa}$
	s"π^0" $\to K^- u(\to K^+)$	$\delta\sqrt{\kappa}\gamma$
	$\bar{s}$"π^0" $\to K^+ \bar{u}(\to K^-)$	$\delta\sqrt{\kappa}\gamma$
	$u\bar{u} \to K^+K^-$	κ
$K^-\pi^+$	$\bar{d}$"π^0" $\to \pi^+ \bar{u}(\to K^-)$	δ
	s"π^0" $\to K^- u(\to \pi^+)$	$\sqrt{\kappa}\gamma$
	u"$\bar{K}^0$" $\to \pi^+ s(\to K^-)$	$\sqrt{\kappa}\alpha$
$K^-\pi^-$	s"π^-" $\to K^- d(\to \pi^-)$	$\gamma\sqrt{\kappa}$
	d"K^-" $\to \pi^- s(\to K^-)$	$\alpha\sqrt{\kappa}$
	$\bar{u}$"π^-" $\to \pi^- \bar{u}$ $(\to K^-)$	δ
K^-K^-	s"K^-" $\to K^- s(\to K^-)$	$\kappa\alpha\gamma$
	$\bar{u}$"K^-" $\to K^- \bar{u}(\to K^-)$	$\kappa\alpha\delta$

cross section is increased to 0.12. These can be compared to the CIM prediction,

$$[\pi^+\pi^-: \pi^-K^+: K^-\pi^+: K^+K^-]_{\text{CIM}} = 1.15 : 0.24 : 0.04 : 0.16. \tag{3.4}$$

The obvious discrepancies are the small size of the $K^-\pi^+$ cross section and (relative to the A-corrected value) the large K^+K^- cross section predicted by the CIM. These discrepancies are directly related to the fact that large quantum-number correlations are inherent in the CIM subprocesses, especially the fusion mechanism which results in $K^-K^+ > K^-\pi^+$.

Another way to characterize these results is in terms of "factorization," which is an indication of the absence of charge correlations. The above data obey

$$[(\pi^+\pi^-)(K^+K^-) : (\pi^-K^+)(K^-\pi^+)]_{\text{expt}} = 0.08 : 0.078, \tag{3.5}$$

where factorization would yield 1:1. Factorization will be typical of the elelmentary QCD subprocesses which will also be shown to yield very little quantum-number correlation. The higher-twist CIM subprocess predictions do not obey factorization.

The above experimental data appear qualitatively different from recent data (obtained only at p_T values slightly below those of the Jöstlein *et al.* experiment) from Finley *et al.*[12] While these latter data are at dangerously low-p_T values for interpretation in the present framework they do show charge correlations and lack of factorization as well as A dependences which are different than those of Jöstlein *et al.* in the region of near overlap. Thus it is certainly too soon drawn any firm conclusions.

Complementary information on quantum-number correlations is provided by the ratio (we use the exact numerical-integration numbers of Table II)

$$R^{\text{given}}_{\text{trigger}} = \left(\frac{\text{No. of opposite-sign charges of equal } p_T \text{ on opposing side}}{\text{No. of same-sign charges of equal } p_T \text{ on opposing side}}\right)^{\text{given}}_{\text{trigger}}. \tag{3.6}$$

We obtain ($p_T = 3$ GeV, $x_T = 0.25$)

$$R^{\text{CIM}}_{\pi^\Phi} = \left(\frac{\pi^+\pi^- + \pi^+K^-}{\pi^+\pi^+ + \pi^+K^+}\right) = 1.4,$$

$$R^{\text{CIM}}_{\pi^-} = \left(\frac{\pi^-\pi^+ + \pi^-K^+}{\pi^-\pi^- + \pi^-K^-}\right) = 4.2, \tag{3.7}$$

$$R^{\text{CIM}}_{K^+} = \left(\frac{K^+K^- + K^+\pi^-}{K^+K^+ + K^+\pi^+}\right) = 1.3,$$

$$R^{\text{CIM}}_{K^-} = \left(\frac{K^-K^+ + K^-\pi^+}{K^-\pi^- + K^-K^-}\right) = 10.0.$$

There are, in fact, preliminary indications that a

TABLE II. Meson pairs in CIM.

Observed pair	Standard relative value [a]	Analytic form
$\pi^+\pi^-$	$1.5 \times 4.3 \times 10^{-8}$ GeV^{-4} $(1.5) \times (4.3 \times 10^{-8}$ GeV$^{-4})$	$0.1\sqrt{2/3}(1+r)(1-x_T)^8 \frac{\bar{I}(x_T,4,1,8)}{p_T{}^{10}}$
	$\frac{0.7}{2.2}$ $\frac{(0.7)}{(2.2)}$	$0.1(0.4+0.4r)(0.0583)\frac{(1-x_T)^{10}}{2\langle k^2\rangle p_T{}^8}$
$\pi^+\pi^+$	1.2 (1.2)	$0.1\sqrt{2/3}(0.5+0.2r)2(1-x_T)^8 \frac{\bar{I}(x_T,4,1,8)}{p_T{}^{10}}$
$\pi^-\pi^-$	0.6 (0.6)	$0.1\sqrt{2/3}(0.1+0.4r)2(1-x_T)^8 \frac{\bar{I}(x_T,4,1,8)}{p_T{}^{10}}$
$K^+\pi^-$	0.46 (0.46)	$0.1\sqrt{2/3}[(0.4+0.1r)\alpha\kappa+(0.3+0.8r)\delta](1-x_T)^8 \frac{\bar{I}(x_T,4,1,8)}{p_T{}^{10}}$
$K^+\pi^+$	0.45 (0.45)	$0.1\sqrt{2/3}[(0.5+0.2r)(\alpha\kappa+\delta)](1-x_T)^8 \frac{\bar{I}(x_T,4,1,8)}{p_T{}^{10}}$
K^+K^+	0.15 (0.15)	$0.1\sqrt{2/3}(0.5+0.2r)2\delta\alpha\kappa(1-x_T)^8 \frac{\bar{I}(x_T,4,1,8)}{p_T{}^{10}}$
K^+K^-	0.015 (0.015)	$0.1\sqrt{2/3}(0.3+0.1r)\alpha'\kappa(0.66)(1-x_T)^{12} \frac{\bar{I}(x_T,4,1,12)}{p_T{}^{10}}$
	0.0619 (0.062)	$0.1\sqrt{2/3}(1.0+0.8r)(1/16)\sqrt{\kappa}(1-x_T)^8 \frac{\bar{I}(x_T,4,1,8)}{p_T{}^{10}}$
	0.018 (0.017)	$0.1\sqrt{2/3}(0.36)\sqrt{\kappa}\delta\gamma(1-x_T)^{12} \frac{\bar{I}(x_T,4,1,12)}{p_T{}^{10}}$
	$\frac{0.201}{0.296}$ $\frac{(0.204)}{(0.298)}$	$0.1(0.3+0.1r)(0.0583)\frac{\kappa(1-x_T)^{10}}{2\langle k^2\rangle p_T^8}$
$K^-\pi^+$	0.042 (0.041)	$0.1\sqrt{2/3}(\delta+\sqrt{\kappa}\gamma)(0.18)(1-x_T)^{12} \frac{\bar{I}(x_T,4,1,12)}{p_T{}^{10}}$
	$\frac{0.023}{0.065}$ $\frac{(0.022)}{(0.063)}$	$0.1\sqrt{2/3}(0.3+0.1r)\sqrt{\kappa}\alpha(0.66)(1-x_T)^{12} \frac{\bar{I}(x_T,4,1,12)}{p_T{}^{10}}$
$K^-\pi^-$	0.019 (0.019)	$0.1\sqrt{2/3}(\gamma\sqrt{\kappa}+\delta)(0.082)(1-x_T)^{12} \frac{\bar{I}(x_T,4,1,12)}{p_T{}^{10}}$
	$\frac{0.016}{0.035}$ $\frac{(0.016)}{(0.035)}$	$0.1\sqrt{2/3}(0.3r+0.1)\alpha\sqrt{\kappa}(0.66)(1-x_T)^{12} \frac{\bar{I}(x_T,4,1,12)}{p_T{}^{10}}$
K^-K^-	0.0017 (0.0015)	$0.1\sqrt{2/3}\kappa\alpha(\gamma+\delta)2(0.043)(1-x_T)^{16} \frac{\bar{I}(x_T,4,1,16)}{p_T{}^{10}}$

[a] This standard relative value is for $p_T = 3$ GeV, $x_T = 0.25$, $\langle k^2\rangle = \langle l^2\rangle = 0.5$ GeV^2, all SU(3)-breaking parameters $(\alpha, \alpha', \delta, \delta', \ldots) = \frac{1}{2}$, and $r = \frac{1}{2}$. ( ) gives numerical result for the analytic form.

strong positive charge excess is seen opposite both a K^- and a π^- trigger in pp collisions.[7,8,13,14] The observed ratios (of the order of 2) are not as large as those computed in Eq. (3.7). This is partly because we have quoted values for exactly symmetric pair production, at which point the fusion mechanism is very important. Also, the calculations given here have not incorporated resonance-production feedthrough [e.g., $q_1 M_1 - K^{*0} q^2$ $(K^{*0} - K^-)$] which will tend to diminish the large ratios. The third, and most important, effect is that presence of other contributions (in particular the elementary QCD subprocess contributions) would decrease the R values. These effects also result in relative cross-section ratios nearer those obtained by Jöstlein *et al.* Below we will make a more quantitative comparison, including the contributions of the elementary QCD processes. We will also estimate the effects of resonances. Qualitatively, the fact that a number of different experiments have yielded $R_{\pi^-,K^-} \gtrsim 2$ is strong support for an approach which considers a mixture of CIM and QCD; the elementary QCD terms alone always predict R values near one.

In order to aid in a comparison between the QCD subprocesses and the CIM subprocesses it is useful to tabulate results for QCD subprocess contributions to meson pairs. These results will

ignore scale breaking and thus can only be regarded as rough approximations. However, for $\alpha_s = 0.15$ it has been shown[5] that the closely related predictions for the p_T^{-4} subprocess contributions to single-particle spectra do a remarkable job of describing the observed transition between the CIM (p_T^{-8} or p_T^{-12}) realm and the QCD (p_T^{-4}) region as p_T increases. Table III presents the QCD contributions for meson pairs. The final SU(3)-breaking parameter appears in this table:

$$\delta' = \frac{d_{K^\pm}/g}{d_{\pi^\pm}/g} . \tag{3.8}$$

For details of QCD parameters and cross section forms see Ref. 5. For totally symmetric pairs we numerically compute J in (2.15); we also (in parentheses) indicate the results obtained from the listed analytic forms (derived in the Appendix). We sum over the elementary subprocessess—$qq \to qq$, $qg \to qg$, and $gg \to gg$ and over all possible fragmentations. Again we tabulate relative cross-section magnitudes at $p_T = 3$ GeV, $x_T = 0.25$ taking all SU(3) parameters $= \frac{1}{2}$, $r = \frac{1}{2}$ and $\langle k^2 \rangle = \langle l^2 \rangle = 0.5$ GeV^2. Note first the ordering of the cross sections

$$\pi^+\pi^+ > \pi^+\pi^- > \pi^-\pi^- > K^+\pi^+ > K^+\pi^- > K^-\pi^+ > K^-\pi^- > K^+K^+ > K^+K^- > K^-K^- , \tag{3.9}$$

which is different from that of the CIM subprocesses. Next we record the values of the R's for QCD alone (numerical-integration results are used):

$$\begin{aligned} R_{\pi^+}^{\rm QCD} &= 0.80 , \\ R_{\pi^-}^{\rm QCD} &= 1.40 , \\ R_{K^+}^{\rm QCD} &= 0.85 , \\ R_{K^-}^{\rm QCD} &= 1.45 . \end{aligned} \tag{3.10}$$

We may also look at the numerical cross-section ratios. The QCD subprocesses yield a prediction

$$[\pi^+\pi^- : \pi^-K^+ : K^-\pi^+ : K^+K^-]_{\rm QCD} = 1.0 : 0.50 : 0.29 : 0.15. \tag{3.11}$$

The relative size of cross sections appears to be in better agreement with the Jöstlein *et al.* experiment than for the CIM, but there is correspondingly little charge correlation. Note that the above QCD predictions are close to obeying factorization

$$[(\pi^+\pi^-)(K^+K^-) : (\pi^-K^+)(K^-\pi^+)]_{\rm QCD} = 0.15 : 0.145 , \tag{3.12}$$

which is indeed an indication of the smallness of correlations in the QCD (p_T^{-4}) subprocess approach.

Of course, in reality, we must consider a combination of CIM and QCD contributions. Within the present framework the numerically obtained absolute normalizations of the cross sections of Tables II and III will be used. Our normalizations imply that the $\pi^+\pi^-$ cross section, at the $p_T = 3$ GeV, $x_T = 0.25$ point, is composed of 73% CIM and of 27% elementary QCD contributions. We thus take the relative values at the standard kinematic point from Tables II and III in the following proportion:

$$\text{Table IV} = \text{Table II} + 0.177\ \text{Table III} . \tag{3.13}$$

For instance,

$$\begin{aligned} \pi^+\pi^- &= 2.2 + 0.177 \times 4.6 \\ &= 2.2 + 0.814 = 3.014 , \end{aligned} \tag{3.14}$$

which yields a QCD $\pi^+\pi^-$ percentage of $0.814/3.014 = 0.27$. We obtain the relative magnitudes of Table IV. We see that with this combination of QCD and CIM one obtains

$$[\pi^+\pi^- : \pi^-K^+ : K^-\pi^+ : K^+K^-] = 1.0 : 0.29 : 0.10 : 0.14 , \tag{3.15}$$

which, of course, is in better agreement with the Jöstlein *et al.* experiment than ratios predicted on the basis of CIM subprocesses alone. We note further that the large charge correlations typical of the CIM have not been shielded by the above combination. In particular we have, from the Table IV relative pN cross sections,

$$\begin{aligned} R_{\pi^+}^{\rm QCD+CIM} &= 1.1 , \\ R_{\pi^-}^{\rm QCD+CIM} &= 2.6 , \\ R_{K^+}^{\rm QCD+CIM} &= 1.1 , \\ R_{K^-}^{\rm QCD+CIM} &= 2.4 . \end{aligned} \tag{3.16}$$

The absolute size of QCD relative to CIM contributions will be pursued shortly. For the moment we simply note that it is possible that the data at $p_T \geq 3$ GeV represents a mixture of these contributions. One must, however, be cautious as some of the resonance feed through effects present in CIM subprocesses will result in both an increase in the $K^-\pi^+$ cross section and a decrease in the R values obtained in the direct-production CIM calculations given earlier. An example is $\bar{u}d \to K^-K^{*0}$ following by K^{*0} decay to π^+ (and π^-). This enhances the $K^-\pi^+$ cross section and decreases quantum-number correlations. It is thus remotely possible that the CIM alone could explain the R values and yield cross-section ratios similar to those of Eq. (3.5). Unfortunately it is difficult to compute the resonance feed-through with precision without a thorough knowledge of high-p_T resonance production. In single-particle spectra it is estimated that indirect production via resonances is responsible for about 20%–50% of the cross section. An extreme esti-

TABLE III. QCD contributions for meson pairs. GeV units ($\alpha_s = 0.15$).

Pair	Subprocess	Standard relative value [a]	Analytic form
$\pi^+\pi^-$	$qq \to qq$	0.93 (1.1)	$1.87(1+r)^2 \times 10^{-6} \frac{\bar{J}_{qq}(x_T)}{p_T{}^5}$
[Absolute value at standard point is 7.2×10^{-9} (3.2×10^{-9})]			
	$qg \to qg$	2.3 (2.16)	$2.86(2+2r) \times 10^{-6} \frac{\bar{J}_{qg}(x_T)}{p_T{}^5}$
	$gg \to gg$	1.37 (1.4) / 4.6 (4.66)	$5.9 \times 10^{-6} \frac{\bar{J}_{gg}(x_T)}{p_T{}^5}$
$\pi^+\pi^+$	$qq \to qq$	0.91 (1.07)	$2.73(1+r) \times 10^{-6} \frac{\bar{J}_{qq}(x_T)}{p_T{}^5}$
	$qg \to qg$	2.69 (2.52)	$2.86(3+r) \times 10^{-6} \frac{\bar{J}_{qg}(x_T)}{p_T{}^5}$
	$gg \to gg$	1.37 (1.4)	$5.9 \times 10^{-6} \frac{\bar{J}_{gg}(x_T)}{p_T{}^5}$
		4.97 (4.99)	
$\pi^-\pi^-$	$qq \to qq$	0.406 (0.53)	$2.73(1+r)r \times 10^{-6} \frac{\bar{J}_{qq}(x_T)}{p_T{}^5}$
	$qg \to gg$	1.92 (1.80)	$2.86(3r+1) \times 10^{-6} \frac{\bar{J}_{qg}(x_T)}{p_T{}^5}$
	$gg \to gg$	1.37 (1.4)	$5.9 \times 10^{-6} \frac{\bar{J}_{gg}(x_T)}{p_T{}^5}$
		3.75 (3.73)	
$K^+\pi^-$	$qq \to qq$	0.47 (0.55)	$\delta(1+r)^2\, 1.87 \times 10^{-6}\, \bar{J}_{qq}(x_T)/p_T{}^5$
	$qg \to qg$	1.15 (1.08)	$[(3+r)\delta + (3r+1)\delta']1.43 \times 10^{-6}\, \bar{J}_{qg}(x_T)/p_T{}^5$
	$gg \to gg$	0.68 (0.70)	$\delta'\, 5.9 \times 10^{-6}\, \bar{J}_{gg}(x_T)/p_T{}^5$
		2.30 (2.33)	
$K^+\pi^+$	$qq \to qq$	0.47 (0.53)	$\delta(1+r)2.73 \times 10^{-6}\, \bar{J}_{qq}(x_T)/p_T{}^5$
	$qg \to qg$	1.34 (1.26)	$(3+r)(\delta+\delta')1.43 \times 10^{-6}\, \bar{J}_{qg}(x_T)/p_T{}^5$
	$gg \to gg$	0.68 (0.70)	$\delta'\, 5.9 \times 10^{-6}\, \bar{J}_{gg}(x_T)/p_T{}^5$
		2.49 (2.49)	
K^+K^+	$qq \to qq$	0.23 (0.27)	$\delta^2(1+r)2.73 \times 10^{-6}\, \bar{J}_{qq}(x_T)/p_T{}^5$
	$qg \to qg$	0.67 (0.63)	$\delta\delta'(3+r)2.86 \times 10^{-6}\, \bar{J}_{qg}(x_T)/p_T{}^5$
	$gg \to gg$	0.34 (0.35)	$\delta'^2\, 5.9 \times 10^{-6}\, \bar{J}_{gg}(x_T)/p_T{}^5$
		1.01 (0.98)	
K^+K^-	$qq \to qq$	0	0
	$qg \to qg$	0.34 (0.31)	$\delta\delta'(3+r)1.43 \times 10^{-6}\, \bar{J}_{qg}(x_T)/p_T{}^5$
	$gg \to gg$	0.34 (0.35)	$\delta'^2\, 5.9 \times 10^{-6}\, \bar{J}_{gg}(x_T)/p_T{}^5$
		0.68 (0.66)	
$K^-\pi^+$	$qq \to qq$	0	0
	$qg \to qg$	0.67 (0.63)	$\delta'(3+r)1.43 \times 10^{-6}\, \bar{J}_{qg}(x_T)/p_T{}^5$
	$gg \to gg$	0.68 (0.70)	$\delta'\, 5.9 \times 10^{-6}\, \bar{J}_{gg}(x_T)/p_T{}^5$
		1.35 (1.33)	

TABLE III. (*Continued.*)

Pair	Subprocess	Standard relative value [a]	Analytic form
$K^-\pi^-$	$qg \to qg$	0.48 (0.45)	$\delta'(3r+1)1.43\times10^{-6}\ \bar{J}_{qg}(x_T)/p_T{}^5$
	$gg \to gg$	0.68 (0.70)	$\delta'\ 5.9\times10^{-6}\ \bar{J}_{gg}(x_T)/p_T{}^5$
		1.16 (1.15)	
K^-K^-	$gg \to gg$	0.34 (0.35)	$\delta'^2\ 5.9\times10^{-6}\ \bar{J}_{gg}(x_T)/p_T{}^5$

$$\bar{J}_{qq}(x_T)=\frac{(1-x_T)^9}{[1-(1-x_T)\frac{1}{4}]^6}\frac{1}{[2(\langle k^2\rangle+\langle l^2\rangle)]^{1/2}};\quad \bar{J}_{qg}=\frac{(1-x_T)^{11}}{[1-(1-x_T)\frac{3}{10}]^7}\frac{1}{[2(\langle k^2\rangle+\langle l^2\rangle)]^{1/2}};$$

$$\bar{J}_{gg}(x_T)=\frac{(1-x_T)^{13}}{[1-(1-x_T)\frac{1}{3}]^8}\frac{1}{[2(\langle k^2\rangle+\langle l^2\rangle)]^{1/2}}$$

[a] See footnote of Table II.

mate of the resonance feedthrough effects upon correlations in the CIM can be obtained by considering (for simplicity) only pion pairs. We consider the following two models:

(a) π pairs are all produced directly in relative proportion as given in Table II.

(b) Only ρ pairs are produced directly and all π *pairs arise indirectly* via ρ decay; e.g., $\pi_1^+\pi_2^-$ comes from

$$(\rho^+ + \rho^0)_1\ (\rho^- + \rho^0)_2 = \rho_1^+\rho_2^- + \rho_1^0\rho_2^- + \rho_1^+\rho_2^0 + \rho_1^0\rho_2^0$$

with the relative ρ-pair cross sections obtained from Table II. [We estimate $\rho^+\rho^0=\frac{1}{2}(\rho^+\rho^+ + \rho^+\rho^-)$, etc.]

The comparison is

$$\left.\frac{\pi^+\pi^-}{\pi^+\pi^+}\right|_{\text{direct}} = \frac{2.2}{1.2} = 1.8 \text{ to } \left.\frac{\pi^+\pi^-}{\pi^+\pi^+}\right|_{\text{resonance}} = \frac{6.85}{6.15} = 1.11\ ,$$

$$\left.\frac{\pi^-\pi^+}{\pi^-\pi^-}\right|_{\text{direct}} = \frac{2.2}{0.6} = 3.7 \text{ to } \left.\frac{\pi^-\pi^+}{\pi^-\pi^-}\right|_{\text{resonance}} = \frac{6.85}{4.96} = 1.38\ . \qquad (3.17)$$

It is clear that the pion charge correlations are considerably reduced in the model where all π's arise indirectly via ρ decay. Including K decays to $K\pi$ we would find that if all K's and π's arose either from ρ or K^* decay, the ratios R_{π^-} and R_{K^-} of (3.7) would be approximately cut in half. This is of course an absolute extreme since the observed π and K pairs arise *at most* only 50% of the time from resonances.

TABLE IV. CIM + QCD (weighting described in text).

	pN	pp
$\pi^+\pi^-$	3.01	2.90
$\pi^+\pi^+$	2.08	2.60
$\pi^-\pi^-$	1.26	0.97
$K^+\pi^-$	0.87	0.92
$K^+\pi^+$	0.89	1.10
K^+K^+	0.33	0.45
K^+K^-	0.42	0.465
$K^-\pi^+$	0.30	0.33
$K^-\pi^-$	0.24	0.215
K^-K^-	0.062	0.062

To complete this discussion of basic results we also present predictions for meson-baryon and baryon-baryon pairs. These appear in Tables V and VI. We have not computed all possible cases, only certain representative choices. Subprocess and distribution function parameters are from Ref. 5, except that for numerics we choose $r=f_{d/p}/f_{u/p}=\frac{1}{2}$. A few more SU(3)-breaking parameters are required for the pK^- case: Analogous to (b) we choose

(e) $f_{B(suu)/d}=\alpha f_{B(duu)/p}$.

In addition we consider (for this one case)

(f) "bad" fragmentation, $u\to K^-$ or $d\to K^-$;

we assume that through resonance mediation this is allowed at the level

$$g_{K^-/u\text{ or }d}=2.$$

This, via Eq. (2.13) introduces an extra β/p_T relative to the standard $u\to\pi^+$ or $d\to\pi^-$ cases.

TABLE V. CIM meson-baryon and baryon-baryon pairs.

Pairs	Subprocess	Standard relative value[a]	Analytic form
$p\pi^-$	$d\text{“}p\text{”} \to pd(\to \pi^-)$	$3.73 \times 0.819 \times 10^{-8}$	$3.0(1+\frac{20}{41}r)\frac{(1-x_T)^6}{p_T{}^{14}}\bar{I}(x_T,6,1,6)$
	+	$(3.73 \times 0.822 \times 10^{-8})$	
	$u\text{“}n\text{”} \to pd(\to \pi^-)$		
	$d\text{“}\pi^0\text{”} \to \pi^- u(\to p)$		
	+		
	$d\text{“}\pi^-\text{”} \to \pi^- d(\to p)$	0.30 (0.24)	$0.06(1+\frac{20}{7}r)\frac{2\langle k^2\rangle(1-x_T)^8}{p_T{}^{12}}\bar{I}(x_T,4,3,8)$
	$d(ud) \xrightarrow{\text{fusion}} \pi^- p$	$\underline{1.10}\ \underline{(1.10)}$	$0.006(1+3r)\frac{(1-x_T)^4}{2\langle k^2\rangle p_T{}^{12}}$
		5.13 (5.07)	
pK^-	$d\text{“}\Sigma^+\text{”} \to ps(\to K^-)$		
	+	0.57 (0.57)	$0.93\alpha(1+\frac{6}{13}r)\frac{(1-x_T)^6}{p_T{}^{14}}\bar{I}(x_T,6,1,6)$
	$u\text{“}\Sigma^0\text{”} \to ps(\to K^-)$		
	$d\text{“}p\text{”} \to pd(\to K^-)$	0.18 (0.18)	$6.57\frac{\beta}{p_T}(1+\frac{1}{2}r)\frac{(1-x_T)^6}{p_T{}^{14}}\bar{I}(x_T,6,1,6)$
	+		
	$d\text{“}\Delta^{++}\text{”} \to pu(\to K^-)$		
	$s\text{“}\pi^0\text{”} \to K^- u(\to p)$	0.007 (0.005)	$0.038\gamma\sqrt{\kappa}\frac{2\langle k^2\rangle(1-x_T)^{12}}{p_T{}^{12}}\bar{I}(x_T,4,3,12)$
	+		
	$s\text{“}\pi^-\text{”} \to K^- d(\to p)$		
	$(ud)\text{“}\pi^0\text{”} \to p\bar{u}(\to K^-)$		
	+		
	$(uu)\text{“}\pi^-\text{”} \to p\bar{u}(\to K^-)$	$\underline{0.09}\ \underline{(0.09)}$	$0.18\delta\frac{(1-x_T)^6}{p_T{}^{14}}\bar{I}(x_T,6,1,6)$
		0.85 (0.85)	
$\bar{p}\pi^+$	$u\bar{p} \xrightarrow{(st)} \bar{p}u(\to \pi^+)$		
	+		
	$d\bar{n} \to \bar{p}u(\to \pi^+)$	0.012 (0.011)	$0.1(1+r)\frac{(1-x_T)^{14}}{p_T{}^{14}}\bar{I}(x_T,6,1,14)$
	$(\bar{u}\bar{d})\text{“}\pi^0\text{”} \to \bar{p}u(\to \pi^+)$		
	+		
	$(\bar{u}\bar{u})\text{“}\pi^+\text{”} \to \bar{p}u(\to \pi^+)$	0.030 (0.028)	$0.38\frac{(1-x_T)^{14}}{p_T{}^{14}}\bar{I}(x_T,6,1,14)$
	$\bar{d}\text{“}\pi^+\text{”} \to \pi^+\bar{d}(\to \bar{p})$	$\underline{0.021}\ \underline{(0.016)}$	$0.041(1-x_T)^{12}\frac{2\langle k^2\rangle}{p_T{}^{12}}\bar{I}(x_T,4,3,12)$
	+	0.063 (0.055)	
	$\bar{d}\text{“}\pi^0\text{”} \to \pi^+\bar{u}(\to \bar{p})$		
$p\bar{p}$	$u\bar{u} \xrightarrow{\text{fusion}} p\bar{p}$		
	+		
	$d\bar{d} \xrightarrow{\text{fusion}} p\bar{p}$	1.90 (1.95)	$0.12(1+\frac{7}{13}r)\frac{(1-x_T)^{10}}{2\langle k^2\rangle p_T{}^{12}}$
	$(ud)\text{“}\pi^0\text{”} \to p\bar{u}(\to \bar{p})$	$\underline{0.016}\ \underline{(0.01)}$	$0.515\frac{(1-x_T)^6}{p_T{}^{16}}2\langle k^2\rangle\bar{I}(x_T,6,3,6)$
	+	1.92 (1.96)	
	$(uu)\text{“}\pi^-\text{”} \to p\bar{u}(\to \bar{p})$		

TABLE V. (*Continued.*)

Pairs	Subprocess	Standard relative value[a]	Analytic form
pp	$u\text{“}p\text{”} \to pu(\to p)$		
	+		
	$d\text{“}\Delta^{++}\text{”} \to pu(\to p)$	0.37 (0.27)	$10.2(1+\frac{72}{143}\gamma)\frac{(1-x_T)^6}{p_T{}^{16}}\bar{I}(x_T,6,3,6)$
	+		
	$u\text{“}n\text{”} \to pd(\to p)$		
	+		
	$d\text{“}u\text{”} \to pd(\to p)$		
$p\bar{p}$	$\bar{d}\text{“}\bar{\Delta}^{++}\text{”} \to \bar{p}\bar{u}(\to \bar{p})$		
	+		
	$\bar{d}\text{“}\bar{p}\text{”} \to \bar{p}\bar{d}(\to \bar{p})$		
	+		
	$\bar{u}\text{“}\bar{p}\text{”} \to \bar{p}\bar{u}(\to \bar{p})$	0.002 (0.001)	$3.1\frac{(1-x_T)^{18}}{p_T{}^{16}}\bar{I}(x_T,6,3,18)$
	+		
	$\bar{u}\text{“}\bar{n}\text{”} \to \bar{p}\bar{d}(\to \bar{p})$		

[a] See footnote of Table II.

We crudely estimate $\beta \simeq \frac{1}{10}$ to $\frac{1}{20}$ GeV. The precise definition of β is

$$D_{K^+/u}=\frac{2\beta d_{\pi^+/u}}{(2\pi\langle k^2\rangle)^{1/2}}\frac{(1-x)^2}{x}. \tag{3.18}$$

Examination of the CIM numerical results of Table V at the standard $p_T=3$ GeV, $x_T=0.25$ point indicates the following:

(1) The cross sections we have computed within the CIM are ordered as

$$\pi^- p > p\bar{p} > K^- p > pp > \pi^+\bar{p} > \bar{p}\bar{p} . \tag{3.19}$$

(2) The $\pi^- p$ absolute cross section at this point and the $\pi^-\pi^+$ absolute cross section are in the ratio

$$[\pi^+\pi^- : \pi^- p]_{\text{CIM}} \simeq 2.0 : 1.0, \tag{3.20}$$

i.e., they are comparable in magnitude. This relative ratio is typical of existing data; more discussion of relative normalizations appears shortly.

(3) The pair cross section for $\bar{p}p$ is very strongly dominated by the fusion subprocess $q\bar{q} \to p\bar{p}$ with consequent strong charge correlations. For instance, for a $\bar{p}$ trigger

$$\left(\frac{\bar{p}p}{p\bar{p}}\right)_{\text{CIM}} \sim 1000 , \tag{3.21}$$

and factorization is violated:

$$[(pp)(\bar{p}\bar{p}) : (\bar{p}p)^2]_{\text{CIM}} = 1 : 5000 . \tag{3.22}$$

Finally we present corresponding analytic results for the QCD subprocess contributions to these same pair cross sections. These appear in Table VI.

Again examining the numerical results at the standard $p_T=3$ GeV, $x_T=0.25$ point we observe the following:

(1) The cross sections are ordered for QCD subprocesses as

$$\pi^- p > pp > \bar{p}\pi^+ > pK^- > p\bar{p} > \bar{p}\bar{p} . \tag{3.23}$$

The $\pi^+\bar{p}$ and $\bar{p}\bar{p}$ cross sections are relatively enhanced compared to the CIM. This is because of the presence of scattered gluons, in the QCD framework, which do not distinguish between quantum numbers. The $p\bar{p}$ cross section is relatively smaller because of the absence of a fusion diagram in QCD.

(2) The $\pi^- p$ and $\pi^-\pi^+$ absolute cross sections from purely $p_T{}^{-4}$ subprocesses are in the ratio

$$[\pi^+\pi^- : \pi^- p]_{\text{QCD}} \simeq 3.1 : 1.0 . \tag{3.24}$$

(3) The charge correlations within QCD are much smaller than those in the CIM:

$$\left(\frac{\bar{p}p}{p\bar{p}}\right)_{\text{QCD}} \sim 3 , \tag{3.25}$$

$$[(pp)(\bar{p}\bar{p}) : (\bar{p}p)^2]_{\text{QCD}} \sim 1.0 : 1.2 . \tag{3.26}$$

As for the meson pairs, indirect resonance feedthrough in CIM processes will tend to modify the predictions given here for the CIM on the basis of direct production. Again these modifications as to correlations, etc., are like those that would result from a mixture of CIM + elementary

TABLE VI. QCD meson-baryon and baryon-baryon.

Pair	Subprocess	Standard relative value [a]	Analytic form
$p\pi^-$	$qq \to qq$	0.92 (1)	$0.407(1+r)(1+1.733r)10^{-6}J'_{qq}(x_T)/p_T^5$
	[Absolute values: 2.39×10^{-9} (1.2×10^{-9})]		
	$qg \to qg$	2.4 (2.4)	$0.208(9+11r)10^{-6}J'_{qg}(x_T)/p_T^5$
	$gg \to gg$	1.2 (1.1)	$1.51\times10^{-6}J'_{gg}(x_T)/p_T^5$
		4.5 (4.5)	
pK^-	$qq \to qq$	0	0
	$qg \to qg$	(0.81)	$\delta'\ 0.208(7+5r)\times10^{-6}J'_{qg}(x_T)/p_T^5$
	$gg \to gg$	(0.55)	$\delta'\ 1.51\times10^{-6}J'_{gg}(x_T)/p_T^5$
		(1.36)	
$\bar{p}\pi^+$	$qq \to qq$	0	0
	$qg \to qg$	(1.1)	$0.383(3+r)\times10^{-6}J'_{qg}(x_T)/p_T^5$
	$gg \to gg$	(1.1)	$1.51\times10^{-6}J'_{gg}(x_T)/p_T^5$
		(2.2)	
$J'_{qq}=\frac{(1-x_T)^{11}}{[1-(1-x_T)^{\frac{2}{5}}]^6}\frac{1}{[2(\langle k^2\rangle+\langle l^2\rangle)]^{1/2}}$,		$J'_{qg}=\frac{(1-x_T)^{13}}{[1-(1-x_T)^{\frac{5}{12}}]^7}\frac{1}{[2(\langle k^2\rangle+\langle l^2\rangle)]^{1/2}}$,	$J'_{gg}=\frac{(1-x_T)^{15}}{[1-(1-x_T)^{\frac{3}{7}}]^8}\frac{1}{[2(\langle k^2\rangle+\langle l^2\rangle)^{1/2}}$
pp	$qq \to qq$	(0.72)	$3.86(1+r)(1+0.554r)\times10^{-7}J''_{qq}(x_T)/p_T^5$
	$qg \to qg$	(1.29)	$1.558(7+5r)\times10^{-7}J''_{qg}(x_T)/p_T^5$
	$gg \to gg$	(0.34)	$5.6\times10^{-7}J''_{gg}(x_T)/p_T^5$
		(2.35)	
$\bar{p}p$	$qq \to qq$	0	0
	$qg \to qg$	(0.65)	$0.779(7+5r)\times10^{-7}J''_{qg}(x_T)/p_T^5$
	$gg \to gg$	(0.34)	$5.6\times10^{-7}J''_{gg}(x_T)/p_T^5$
		(0.99)	
$\bar{p}\bar{p}$	$qq \to qq$	0	0
	$qg \to qg$	0	0
	$gg \to gg$	(0.34)	$5.6\times10^{-7}J''_{gg}(x_T)/p_T^5$
$J''_{qq}(x_T)=\frac{(1-x_T)^{13}}{[1-(1-x_T)^{\frac{1}{2}}]^6}\frac{1}{[2(\langle k^2\rangle+\langle l^2\rangle)]^{1/2}}$,		$J''_{qg}=\frac{(1-x_T)^{15}}{[1-(1-x_T)^{\frac{1}{2}}]^7}\frac{1}{[2(\langle k^2\rangle+\langle l^2\rangle)]^{1/2}}$,	$J''_{gg}=\frac{(1-x_T)^{17}}{[1-(1-x_T)^{\frac{1}{2}}]^8}\frac{1}{[2(\langle k^2\rangle+\langle l^2\rangle)]^{1/2}}$

[a] See footnote of Table II.

QCD. The important point is that elementary QCD subprocesses alone predict an almost complete absence of charge correlations.

We now turn to a more detailed discussion of charge correlations for meson pairs. The existing experiments employ pp collisions. This tends to increase the CIM charge correlations. For instance, at our standard symmetric point $x_T = 0.25$, $p_T = 3$ GeV we may use Table VII (with $r=\frac{1}{2}$) to convert the pN Table II results to pp results. The relative normalizations are altered somewhat. This yield R^{CIM} values as follows:

$$\begin{aligned} R_{\pi^+}^{\mathrm{CIM}} &= 1.0\ , \\ R_{\pi^-}^{\mathrm{CIM}} &= 5.8\ , \\ R_{K^+}^{\mathrm{CIM}} &= 0.9\ , \\ R_{K^-}^{\mathrm{CIM}} &= 13.8\ . \end{aligned} \tag{3.27}$$

Again we remind the reader that resonance feedthrough and presence of elementary QCD terms will reduce the large R_{π^-} and R_{K^-} values. The effects of QCD terms can be established by taking the new relative QCD values computed in Table VII and forming the superposition (3.16) which cor-

TABLE VII. Conversion table for pN to pp collisions.

(Meson pairs)						
	CIM		New		QCD	New
	pN	pp	relative value	pN	pp	relative values
$\pi^+\pi^-$	$(1+r)$	$(0.8+1.2r)$	2.1	$(1+r)^2$	$4r$	0.827
	$(0.4+0.4r)$	$(0.4+0.4r)$		$2(1+r)$	$2(1+r)$	2.3
				1	1	1.37
						4.50
$\pi^+\pi^+$	$(0.5+0.2r)$	0.8	1.6	$(1+r)$	2	1.21
				$(3+r)$	4	3.07
				1	1	1.37
						5.65
$\pi^-\pi^-$	$(0.1+0.4r)$	$0.4r$	0.4	$r(1+r)$	$2r^2$	0.307
				$(3r+1)$	$4r$	1.536
				1	1	1.37
						3.21
$K^+\pi^-$	$(0.4+0.1r)$	0.4	0.4	$(1+r)^2$	$4r$	0.42
	$(0.3+0.8r)$	$1.2r$		$(3+r)$	4	1.15
				$(3r+1)$	$4r$	
				1	1	1.37
						2.94
$K^+\pi^+$	$(0.5+0.2r)$	0.8	0.6	$(1+r)$	2	0.61
				$(3+r)$	4	1.53
				1	1	0.68
						2.82
K^+K^+	$(0.5+0.2r)$	0.8	0.2	$(1+r)$	2	0.30
				$(3+r)$	4	0.77
				1	1	0.34
						1.41
K^+K^-	$(0.3+0.1r)$	0.4	0.017	0	0	0
	$(1+0.8r)$	$(1.2+0.8r)$	0.071	$(3+r)$	4	0.38
	0.36	$\frac{36}{33}$ (0.36)	0.0195	1	1	0.34
						0.72
	$(0.3+0.1r)$	0.4	0.23			
			0.338			
$K^-\pi^+$	0.18	(0.18) $\frac{36}{33}$	0.046	0	0	0
				$(3+r)$	4	0.77
	$(0.3+0.1r)$	0.4	0.026	1	1	0.68
			0.072			1.45

TABLE VII. (*Continued.*)

(Meson pairs)	CIM		New relative	QCD		New relative
	pN	pp	value	pN	pp	values
$K^-\pi^-$	0.082	$(0.082)\frac{6}{7.5}$	0.015	0	0	0
				$(3r+1)$	$4r$	0.38
	$(0.3r+0.1)$	$0.4r$	0.013	1	1	0.68
			0.028			1.06
K^-K^-	0.043	0.043	0.0017	1	1	0.34

rectly accounts for the predicted relative absolute normalizations. The results are tabulated in Table IV. We obtain for pp collisions

$$\begin{aligned} R_{\pi^+}^{\mathrm{CIM+QCD}} &= 0.87 , \\ R_{\pi^-}^{\mathrm{CIM+QCD}} &= 3.2 , \\ R_{K^+}^{\mathrm{CIM+QCD}} &= 0.89 , \\ R_{K^-}^{\mathrm{CIM+QCD}} &= 2.7 . \end{aligned} \tag{3.28}$$

Note that by combining CIM and QCD subprocesses the large value of R_{K^-} has been reduced, so that $R_{K^-} \sim R_{\pi^-}$. That R_{K^-} is reduced more than R_{π^-} is due to the fact that the CIM contributions to K^- production require sea quarks and are thus much smaller than CIM contributions to π^- production. Therefore these contributions are more strongly shielded by the QCD terms, especially $gg \to gg$, which contribute roughly equally to π^- and K^-. By comparing (3.16) to (3.28) we see that charge correlations for negative triggers in pp collisions are expected to be even larger than in pN collisions.

The existing experiments do not use a symmetric momentum point. Only for the Albrow *et al.*[7] experiment do we have a good idea of the relative size of p_T^1 and p_T^2. There we have

$$\begin{aligned} p_T^1 &= 3 \text{ GeV}/c , \\ p_T^2 &= 1.5 \text{ GeV}/c . \end{aligned} \tag{3.29}$$

We have used numerical integration to evaluate both the CIM and elementary-QCD meson-pair cross sections in pp collisions at this asymmetric point. The results for the R's including both contributions are shown in Fig. 3. The general features of the data are reproduced. The R_{π^-} value predicted by the theory is above the data; this is probably due, in part, to our not including resonance feedthrough effects which will cause R_{π^-} to decrease. R_{K^-} is less effected by resonance feedthrough.

We have also computed the R's at the Fermilab energy 200 GeV. We have chosen $p_T^1 = 3$ GeV/c and $p_T^2 = 1.2$ GeV/c. This ratio corresponds to the $x_E = 0.4$ cut employed by Bromberg *et al.*[8] in plotting their R values. We do not know, however, if the $p_T^1 = 3$ GeV/c cut is appropriate. Nonetheless, we plot our QCD+ CIM results and their experimental R values on the same figure, Fig. 4. (Note that their R_{π^+} and R_{K^+} are the inverse of ours.) Clearly the predicted R_{π^-} and R_{K^-} values are too high unless

(a) the actual p_T^1 cut is much lower and uncorrelated backgrounds are present, or

(b) resonance effects are much more significant than we expect.

We next turn to a comparison with the beryllium data of Jöstlein *et al.*[6] at a more detailed level. In Fig. 5 we give our absolute prediction for $\pi^+\pi^-$ pair production at $p_{\mathrm{lab}} = 400$, 300, and 200 GeV as a function of

$$x_T = \frac{p_T^s}{\sqrt{s}} , \quad p_T^s = p_T^{\pi^+} + p_T^{\pi^-} .$$

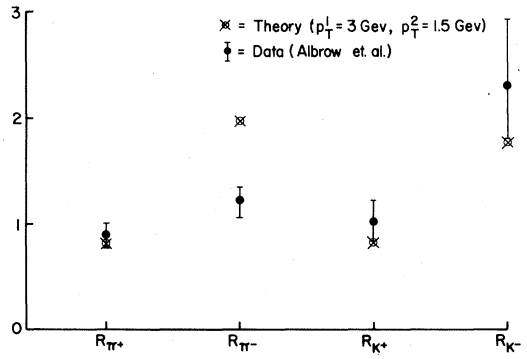

FIG. 3. Plot of experimental points and theoretical predictions for R [defined in Eq. (3.7)]. Data are from Albrow *et al.*—Ref. 7. Theoretical calculations use the $p_T^1 \sim 3$ GeV/c, $p_T^2 \sim 1.5$ GeV/c cuts of the experiment.

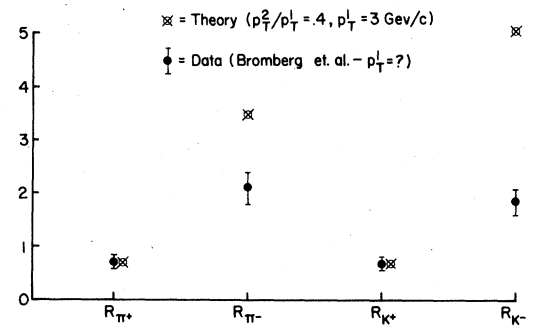

FIG. 4. Plot of R, Eq. (3.7); data from Bromberg *et al.* Theoretical points presume $x_E = 0.4$ and $p_T^1 = 3$ GeV/c. The cuts of the experiment have not been published. Our R_{π^+} and R_{K^+} are the inverse of those defined by Ref. 8.

Both CIM and QCD contributions (obtained by exact numerical integration) are included. We have used pointlike A dependence, that is, we multiply our pN cross section by a factor of 9. (The measured A dependence of the experiment is near 1; however, one must be cautious as the A dependence obtained by the Finley *et al.*[12] at low p_T is different.) We see that the shape and relative normalizations of the three energies are excellent; our prediction is a uniform factor of 1.5–2.0 too high. This is well within the errors which one should assign to our fundamental coupling strengths

$$\alpha_M = 2 \text{ GeV}^2, \quad \alpha_s = 0.15. \tag{3.30}$$

It is perhaps worth noting that the CIM alone is in complete agreement with the data shown. The QCD contributions can be said to cause the normalization to be too high.

In Fig. 6 we display the experimental points and QCD+CIM predictions for the dependence of the $\pi^+\pi^-$ spectrum on the difference $p_T' = p_T^{\pi^+} - p_T^{\pi^-}$ between the momenta of the π^+ and π^-. The weak dependence of the data on p_T' is reproduced. We plot this dependence for other pairs as well. In Fig. 7 we compare predicted and measured $p_T' = p_T^{K^+} - p_T^{\pi^-}$ dependence for various $p_T^s = p_T^{K^+} + p_T^{\pi^-}$ values. Again agreement in shape is generally good. Note that the absolute cross-section value is also very good (using linear A dependence). Figure 8 shows corresponding results for π^+K^- pairs with generally good agreement. Finally Fig. 9 exhibits the corresponding spectra for $p^+\pi^-$ pairs. The theoretical curves are in excellent agreement with experiment for $p_T' = p_T^p - p_T^{\pi^-} < 0$ but tend to lie above the data for $p_T' > 0$. This can be traced to the dominance of the CIM contribution in which an initial proton (or neutron) emits (with ease) a secondary baryon which then produces directly (via the $Bq \to pq'$ subprocess) the observed proton. The proton is obviously made with a higher momentum than the symmetric π-produced in the decay of the q'. For negative p_T' the reverse process $Mq \to \pi q'$ ($q' \to p$) which

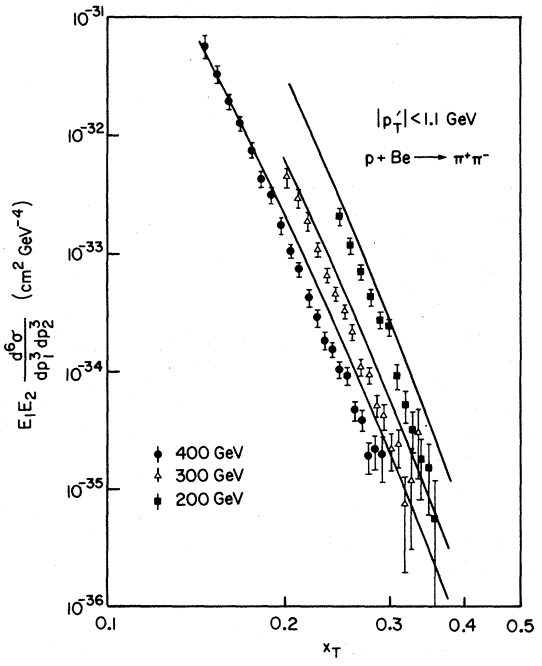

FIG. 5. Comparison of QCD+CIM theoretical curves with the data (Ref. 6) of Jöstlein *et al.* for $\pi^+\pi^-$ pairs, as a function of $x_T = (p_T^{\pi^+} + p_T^{\pi^-})/\sqrt{s} \equiv p_T^s/\sqrt{s}$.

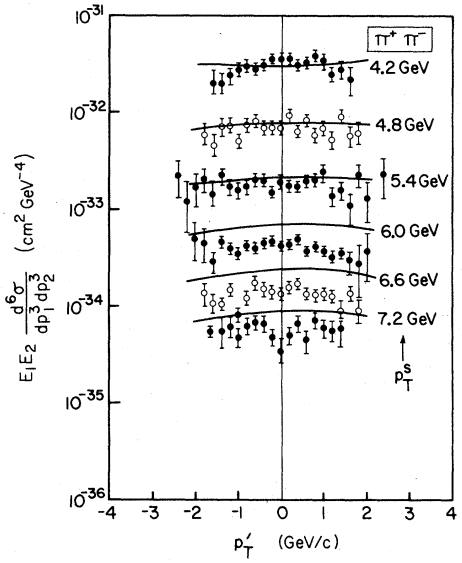

FIG. 6. As in Fig. 5 except that the absolute normalization and dependence on $p_T' = p_T^{\pi^+} - p_T^{\pi^-}$ is compared for various values of p_T^s.

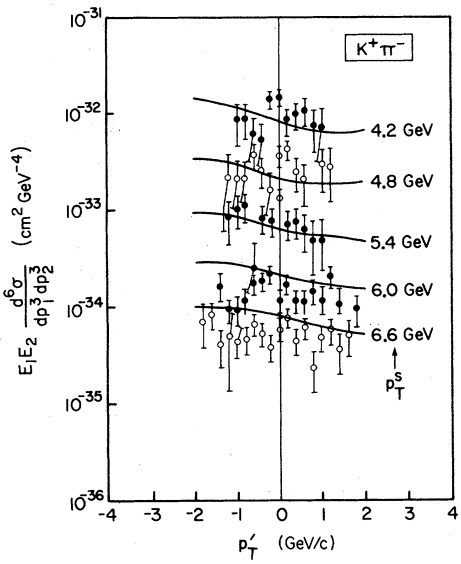

FIG. 7. As in Fig. 6 for $K^+\pi^-$ pairs; $p'_T = p_T^{K^+} - p_T^{\pi^-}$.

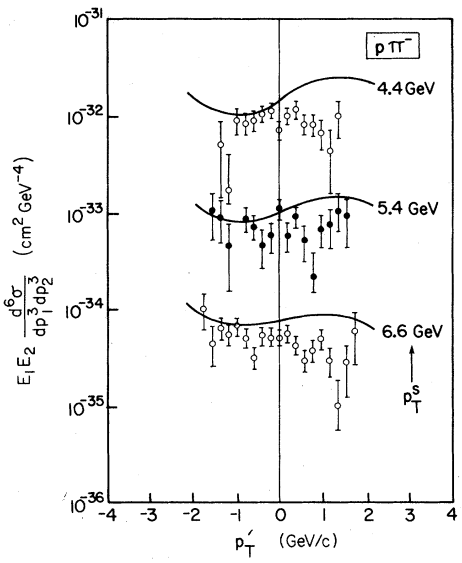

FIG. 9. As in Fig. 6 except for $p\pi^-$ pairs.

favors $p_T^{\pi^-} > p_T^{p}$ becomes significant and agrees well with the data. Conceivably our choice of

$$\alpha_B = 10 \text{ GeV}^4 , \tag{3.31}$$

which normalizes the $Bq \to pq'$ subprocess, is a bit too large. Certainly a 20% adjustment is within the errors allowed by earlier determinations and single-particle spectra fits. We also note that the $p\pi^-$ pair spectrum is dominated by the CIM terms. The QCD contributions are much smaller than the data in this region; for $p_T^s = 4.4$ GeV they are a factor of 4 to 8 below the data.

Overall the predicted spectra are in surprisingly good agreement with the experimental observations. The theory has certain intrinsic uncertainties which render absolute normalization calculations to better than 50% impossible. In addition we have chosen our SU(3)-breaking parameters $\alpha' = \alpha = \delta = \ldots = \frac{1}{2}$ on the basis of reasonableness rather than direct experimental determination.

Unfortunately on the basis of the Jöstlein *et al.* data a clear case for the presence of only QCD or only CIM subprocesses or a mixture, as used here, cannot be made.

The QCD+CIM mixture predicts values for n_{eff} for $\pi^+\pi^-$ pairs at $x_T = 0.15$ as follows:

$$\begin{aligned} n_{eff}^{\text{QCD+CIM}} \ (\sqrt{s} = 19.4 \text{ to } \sqrt{s} = 23.7) &= 9.46 , \\ n_{eff}^{\text{QCD+CIM}} \ (\sqrt{s} = 23.7 \text{ to } 27.4) &= 8.77 , \end{aligned} \tag{3.32}$$

whereas CIM alone would predict

$$\begin{aligned} n_{eff}^{\text{CIM}} \ (\sqrt{s} = 19.4 \text{ to } \sqrt{s} = 23.7) &= 9.84 , \\ n_{eff}^{\text{CIM}} \ (\sqrt{s} = 23.7 \text{ to } 27.4) &= 9.5 . \end{aligned} \tag{3.33}$$

Clearly as $\sqrt{s}$ increases at fixed x_T the QCD terms if present should substantially alter the power of $p_T^{-(9\pm0.5)}$ expected on the basis of the CIM. Certaintly if only QCD were present the n_{eff} value should lie below 8. Smearing in k_T should not effect this difference. The experimental value (for $x_T \geq 0.17$)

$$n_{eff}^{\text{expt}} \approx 8.7 \tag{3.34}$$

is perhaps already a bit larger than is comfortable for pure QCD. The above experimental n_{eff}^{expt} averages over data which includes 200-GeV

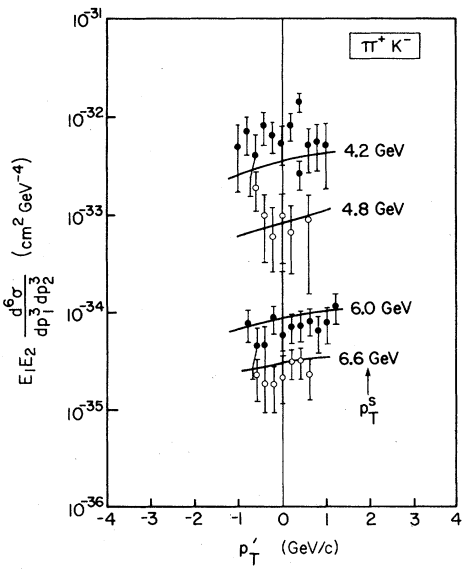

FIG. 8. As in Fig. 6 except for π^+K^- pairs.

data at $y \neq 0$. Correcting for the y dependence (which increases the difference between the p_{lab} = 200 and 300 GeV data) yields an n_{eff} value > 9.2. To clarify the situation very precise measurements on a proton target and/or measurements over a larger energy range would be very useful. Note also that the difference in p_T dependence between CIM and elementary QCD for pairs involving baryons is considerably larger. Thus measurements of, for example, $p\pi^-$ pairs over a larger kinematic range will be interesting.

Next we turn to a consideration of the dN/dx_E distribution—in this paper our z is identical to x_E. The CIM subprocess predictions are quite different from those obtained from elementary QCD subprocesses. We illustrate the basic features by comparing $\pi^+\pi^-$ and $\pi^-\pi^-$ dN/dx_E distributions in Fig. 10. For $\pi^-\pi^-$ pairs the fusion contribution is zero when π's are directly made in the subprocess. Fusion contributions through indirect modes, such as $q\bar{q} \to \pi^-\rho^0$ ($\rho^0 \to \pi^-$) are quite small. In any case these indirect terms yield a dip structure at $x_E = 1$. Thus for $\pi^-\pi^-$ pairs we predict a dip coming from the transverse restrictions on the $qM \to Mq$ ($q \to M'$) CIM contributions near $x_E = 1$. In contrast $\pi^-\pi^+$ pairs have a strong fusion contribution which fills in this dip and even creates a bump at $x_E = 1$ in the dN/dx_E distribution. The normalization of the fusion relative to the other CIM contributions is proportional to $1/\langle k^2 \rangle$ but otherwise completely fixed.

Elementary QCD subprocesses in contrast predict nearly identical dN/dx_E spectra for $\pi^-\pi^-$ $\pi^+\pi^-$ and, unless a large peak in the quark (or gluon) decay function occurs at $z = 1$, will yield (even in the absence of k_T fluctuations) a completely structureless curve near $x_E = 1$. (The nonvanishing "flat" forms used by Feynman and Field[2] are not sufficient to produce structure.) Such a distribution peak has not been observed in the SPEAR-DORIS measurements of quark decay distributions. In Fig. 10 we also plot the prediction for the $\pi^+\pi^-$ dN/dx_E spectrum obtained by combining elementary QCD and CIM subprocesses. The $x_E = 1$ structure becomes very difficult to see at the particular $p_T = 7$ GeV/c trigger value chosen. At lower trigger p_T's the QCD terms should be relatively smaller and any CIM $x_E \sim 1$ structure easier to resolve. (Note that we have arbitrarily normalized the dN/dx_E curves in Fig. 10 to best display the differences in structure.)

There are in fact some recent experimental measurements[15] of dN/dx_E in $\pi^0\pi^0$ pair production

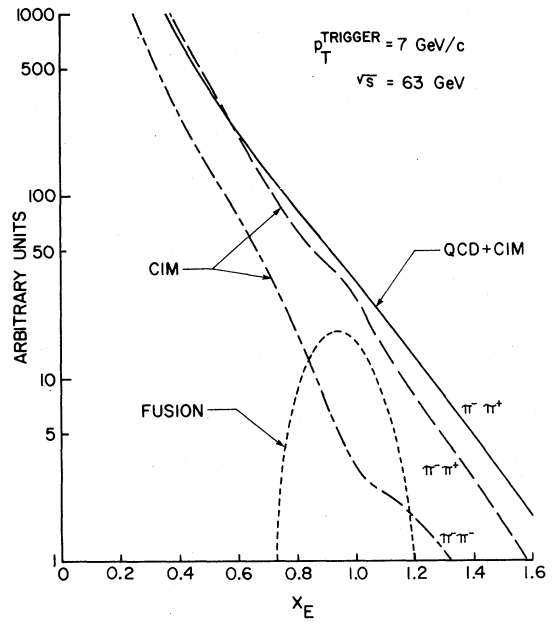

FIG. 10. The dN/dx_E spectrum predicted in the CIM for $\pi^+\pi^-$ pairs compared to $\pi^-\pi^-$ pairs, at a trigger momentum for one pion of 7 GeV/c and for $\sqrt{s} = 63$ GeV. Normalizations of the curves relative to one another are arbitrary and chosen for ease of shape comparison. The fusion contribution to $\pi^+\pi^-$ is shown separately. Also shown is the effect of including QCD terms in the $\pi^-\pi^+$ case.

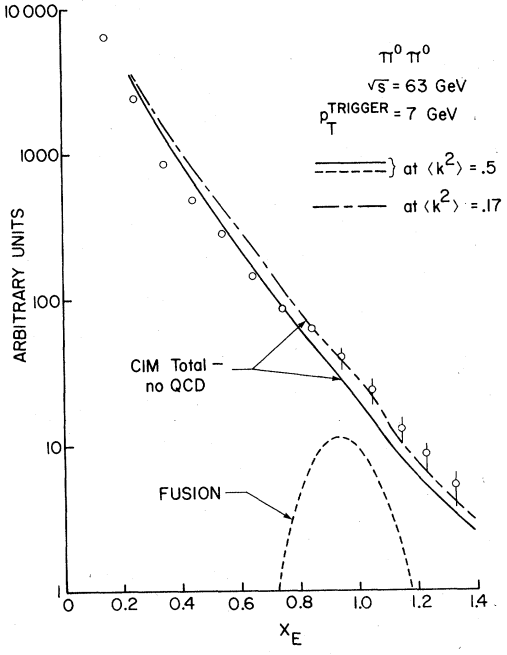

FIG. 11. Comparison of CIM dN/dx_E spectra for $\pi^0\pi^0$ pairs to recent ISR data (Ref. 14) at $\sqrt{s} = 63$ GeV. The structure of the data is larger than that produced by CIM. Including QCD terms weakens the predicted structure further. Absolute normalization of the curves was chosen for ease of comparison to shape of data. Relative normalization of the curves is that given by the theory.

at the ISR which indicate a structure near $x_E = 1$. We have, in Fig. 11, plotted the expectations for dN/dx_E from CIM terms alone (arbitarary over all normalization) compared to data for several different $\langle k^2 \rangle$ values. The fusion contribution just manages to fill the dip coming from the other CIM terms and produces a very slight structure compared to that observed. Elementary QCD contributions (which should be present in substantial proportion) should mask this structure. However, there is a background (which the experimentalists are unable to subtract) coming from direct γ production [as well as $\pi^0 \to \gamma(\gamma)$ they also trigger on a single direct γ]. Thus mechanisms such as $gq \to \gamma q$ $(q \to M)$, $Mq \to \gamma q$ $(q \to M)$, $q\bar{q} \to \gamma M$, etc., are all potentially significant. We will address this problem elsewhere.[16]

Next we consider extrapolation of our $\pi^0\pi^0$ cross section to large-p_T values at $\sqrt{s} = 63$ and 53 GeV. In Fig. 12 the predicted mixture of QCD and CIM is compared to earlier results obtained on the basis of scale breaking of naive QCD terms. The exact scaling of the QCD calculation presented here is certainly too naive and should only be used to indicate approximate trends. In Fig. 12 we also plot the CIM contribution alone, which lies about a factor of 3 below the predictions of Ref. 4 from scale-broken QCD. A reasonable procedure in this realm is to add the CIM predictions (which will be only slightly affected by inclusion of scale breaking) to the scale-broken QCD distributions plotted from Ref. 4. Certainly the indicted range of possibilities brackets the preliminary data obtained at the ISR.[17] These data have substantial absolute normalization error.

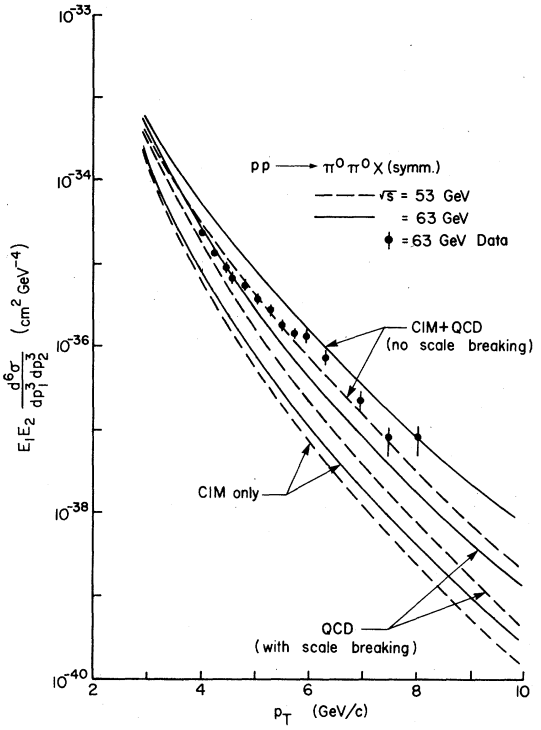

FIG. 12. Double-differential cross section for production of exactly back-to-back $\pi^0\pi^0$ pairs at 90° cm. Three sets of curves are shown. One corresponds to the total CIM contribution alone; the second to the sum CIM+QCD discussed in the text—scale breaking is not included in the QCD terms; the third set of curves shows the scale-broken QCD calculations of Ref. 4. Data are preliminary—presented by Jacob at EPS meeting, Geneva, 1979 (Ref. 17). Since the data presented by Jacob are integrated over the azimuthal-angle difference $(\phi_{\pi_1^0} - \phi_{\pi_2^0})$ we have corrected by multiplying it by the theoretically obtained factor of $\simeq [\sqrt{2\pi}(\langle k^2 \rangle + \langle l^2 \rangle)^{1/2}/p_T]^{-1}$.

IV. CONCLUSION

In this paper we have concentrated on a study of production cross sections for a pair of high-p_T particles—one on each side of the center-of-mass axis. This configuration is important since hard-scattering models for such symmetric-pair cross sections are insensitive to the transverse-momentum fluctuations of the colliding constituents (mesons, quarks, gluons,...). Even the approach,[2] which employs on-shell kinematics for the subprocess so that the fluctuations yield large "smearing" corrections to single-particle spectra, predicts very little "smearing" alteration in the case of symmetric-pair production.[4] Thus the scaling power laws for pair cross sections predicted by the constituent-interchange subprocesses and by the elementary two-body scattering QCD subprocesses can be compared without ambiguity. We have demonstrated that the CIM and elementary QCD contributions yield the following scaling laws at fixed $x_T = (p_T^1 + p_T^2)/\sqrt{s}$, $p_T^1 - p_T^2$ small:

subprocess	Scaling law	
CIM $qM \to qM_1$ (with $M \to M_2$)	$1/p_T^{10}$	Meson pairs
$qM \to M^* q$ (with $M^* \to M_1 M_2$)	$1/p_T^{9}$	Meson pairs
$q\bar{q} \to M_1\bar{M}_2$	$1/p_T^{8}$	Meson pairs

subprocess	Scaling Law	
$qB' \to qB$ (or M)	$1/p_T^{14}$	Baryon-meson pair
$qM \to qM$ (or B)	$1/p_T^{14}$	
$qB' \to qB_1$ (or B_2)	$1/p_T^{16}$	Baryon-(anti)baryon pairs
$q\bar{q} \to B_1\bar{B}_2$	$1/p_T^{12}$	
QCD $qq \to qq$	$1/p_T^5$	
$qg \to gq$		All pairs
$g \to gg$		

Scale breaking will increase the effective power of the elementary QCD subprocesses to at most

$$\text{QCD} \sim (1/p_T)^{7 \text{ or } 8}$$

while having a much smaller effect on the CIM contributions which involve color-singlet amplitudes and distribution functions. Thus a significant difference of 1 to 2 powers in the scaling laws for meson pairs is predicted between CIM and elementary QCD subprocesses; a much larger difference is expected for pairs in which one or both particles are baryons. The pion pair data of Jöstlein *et al.*[6] (especially after correction of the 200-GeV/c data for its nonzero rapidity) appear to indicate a power larger than 9 and consistent with CIM expectations. Indeed, the absolute normalizations we employ for CIM and QCD contributions imply that the CIM terms should dominate the pion-pair data obtained by Jöstlein *et al.* at moderate p_T and $\sqrt{s} = 17$ to 24 GeV. Of course, both the CIM and elementary QCD normalizations should be regarded as uncertain to within a factor of 2. For instance, Baier *et al.*[4] use a larger value of α_s and obtain a satisfactory fit to the pion pair spectra from QCD alone. It is also true, however, that the scale-broken QCD scaling law is not quite the same as that of the experiment. Thus the CIM alone yields an even better description, in normalization and shape, of this data. Adding QCD terms results in a net cross section which in absolute normalization is a bit too high. (Of course, the absolute normalization of the data is very sensitive to small differences in the A dependence assumed.) The $p\pi^-$ pair data present a cleaner situation. Our calculated QCD subprocess contributions lie a factor of 4 to 8 below the Jöstlein *et al.* experiment at $p_T^s = p_T^p + p_T^\pi = 4.4$ GeV/c while CIM terms predict correctly the normalization and shape of the cross section. The QCD subprocess calculations of Baier *et al.*[4] lie a factor of 3 increasing to 8 below the $p_T^s = 4.4$-GeV data as $p_T' = p_T^p - p_T^\pi$ increases from 0 to 2 GeV/c.

Of course, as p_T increases at fixed x_T or fixed $\sqrt{s}$ the elementary QCD terms will become more prominent. For instance, at $p_{\text{lab}} = 400$ GeV/c, without scale breaking, we have the following crossover points at which QCD = CIM:

$\pi^+\pi^-$: $p_T \sim 4.5$ GeV/c,

π^+K^-: $p_T \sim 2$ GeV/c,

$K^+\pi^-$: $p_T \sim 3$ GeV/c,

K^+K^-: $p_T \sim 5$ GeV/c,

$p\pi^-$: $p_T \sim 4$ GeV/c.

Scale breaking will cause an increase in these values and, in general, makes the CIM and elementary QCD spectra more similar in shape.

A particularly important feature of the CIM subprocesses is that they predict large charge (and other quantum-number) correlations. Typical of such correlations are the large "fusion" contributions ($q\bar{q} \to M\bar{M}$ or $B\bar{B}$) which are among the CIM contributions to $\pi^+\pi^-$ pairs and dominate K^+K^- and, especially, $p\bar{p}$ pair production at moderate p_T; fusion contributes only indirectly (through resonances) to $\pi^-\pi^-$ and K^-K^- and is negligible for pp pair cross sections. In contrast quantum-number correlations are predicted to be almost completely absent when the elementary QCD subprocesses alone are used. Typically current data exist in kinematic regions where we expect a mixture of elementary QCD and CIM subprocess contributions; this mixture predicts that charge correlations opposite a π^-, K^-, or $\bar{p}$ trigger are moderate-

ly large. Such correlations are observed in a variety of experiments. Quantitative agreement with the charge correlation results of Albrow *et al.*[7] is a natural consequence of the relative normalizations of the QCD and CIM terms at the appropriate kinematic point. These data represent a coarse measure of the detailed pair spectra for all meson-pair types as obtained here. We have also given predictions for meson-baryon and baryon-baryon pairs. An experimental comparison of $\bar{p}\bar{p}$, $\bar{p}p$, and pp symmetric pairs over a substantial kinematic range will provide an even clearer demonstration of CIM correlations, if present at the expected level.

Another way of exposing these charge correlations and particularly the fusion contributions of the CIM is through the dN/dx_E spectrum. We showed that, if CIM dominates, dN/dx_E should exhibit a dip near $x_E = 1$ for $\pi^-\pi^-$ production, while for $\pi^+\pi^-$ production the addition of the fusion term causes a small bump to appear. Unfortunately even a relatively modest contribution from elementary QCD will obscure the CIM structure; the QCD terms alone predict a smooth dN/dx_E spectrum even if the fragmentation functions of the quarks and gluons do not vanish as $z \to 1$. Thus it is important that the $\pi^+\pi^- - \pi^-\pi^-$ comparison be done at modest p_T and energy.

Finally, though we have not dealt with it in detail here, we recall the importance of measuring the momentum accompanying a trigger particle. For single-particle triggers CIM subprocesses predict a very small amount coming entirely from resonance production and decay. Indeed, 25% to 50% of the momentum observed accompanying a single-meson trigger of moderate p_T has been shown[14] to reside in well-known resonance decay products. Some portion of the remainder is accounted for by background from the beam and target jets. Certainly the nontrivial accompanying momentum is less than 10% of the trigger momentum. Even including k_T-fluctuation smearing this figure remains very uncomfortable for QCD subprocess models. Similar contrasts are present in the symmetric-pair situations. Because smearing, and the resulting bias towards the trigger, is not important in pair production, QCD subprocesses predict that a much larger percentage of the momentum of a trigger will be carried by accompanying particles for a pair trigger. Here we used numerical methods to obtain quantitative estimates as follows. Neglecting scale breaking, one finds that as the transverse momentum of each of two symmetric π^0's increases from 4 to 8 GeV/c (at $\sqrt{s} = 63$ GeV), the accompanying momentum on each side goes from 48% down to 36%. Including scale breaking, one obtains somewhat smaller percentages: ~40% at $p_T^{\pi^0} = 4$ GeV/c down to ~30% at $p_T^{\pi^0} = 8$ GeV/c. The CIM contributions yield a much smaller increase when going from the single-particle to the symmetric-pair trigger. A precise percentage requires more complete knowledge of contributing resonances; certainly it should remain below 15%. For large p_T a mixture of QCD and CIM contributions will be present yielding an intermediate result. Certain triggers, such as K^- and $\bar{p}$, for which QCD terms are relatively large compared to CIM terms at high p_T, should exhibit the largest percentage of momentum accompanying trigger particles.

In summary, it is apparent that the study of high-p_T symmetric pairs will provide a fruitful testing ground for theories of high-transverse-momentum production. A careful study of scaling laws and correlations should indicate a transition from large-inverse-p_T scaling powers to smaller powers and from large-quantum-number correlations to small ones as p_T increases and the elementary QCD subprocesses overtake the higher-twist CIM subprocesses.

ACKNOWLEDGMENTS

We would like to thank SLAC, DESY, and CERN for hospitality during the course of this work. We thank S. Brodsky, R. Blankenbecler, and M. Jacob for helpful discussions. One of us, J. F. G., gratefully acknowledges the support of the U. S. Department of Energy and of the Alfred P. Sloan Foundation.

APPENDIX

In this appendix we will derive the expressions used in the numerical calculations and the analytic approximations mentioned in the text.

We treat separately the three cases illustrated in Figs. 2(a)–2(c). In the first, no fragmentation case, formula (2.1) simplifies to

$$E_C E_D \frac{d\sigma}{d^3p_C d^3p_D} = \frac{s}{2\pi} \int dx_a\, dx_b\, d^2k_a\, d^2k_b \times x_a G_{a/A}(x_a, k_a)\, x_b G_{b/B}(x_b, k_b) \times \frac{d\sigma^{ab\to CD}}{d\hat{t}}\, \delta^4(p_a + p_b - p_C - p_D)\,. \quad \text{(A1)}$$

We will assume that both C and D are produced at 90° in the center of mass and that all momenta of A, B, C, and D lie in the same plane, i.e., $p_{\text{out}}^D = 0$ where p_{out}^D is the momentum component of D perpendicular to the p_A, p_B, p_C plane. We may

parametrize, at large s and p_T, the momenta as

$$\begin{aligned}
&\vec{p}_a = (k_a^x,\ k_a^y,\ x_a \tfrac{1}{2}\sqrt{s}) ,\\
&\vec{p}_b = (k_b^x,\ k_b^y,\ -x_b \tfrac{1}{2}\sqrt{s}) ,\\
&\vec{p}_C = (p_T, 0, 0) ,\\
&\vec{p}_D = (-z p_T, 0, 0) .
\end{aligned} \tag{A2}$$

We assume that $|\vec{p}_T^{\,D}| \leq |\vec{p}_T^{\,C}|$. The momentum components of the δ^4 function yield

$$\begin{aligned}
&k_a^y + k_b^y = 0,\\
&k_a^x + k_b^x = (1-z)p_T ,\\
&x_a = x_b .
\end{aligned} \tag{A3}$$

We use a Gaussian form in the transverse $\vec{k}$ fluctuations as defined in formula (2.2). For p_T large, and z near one, we can neglect the transverse fluctuations in the energy component of the δ^4 function; we can then do the integrals over $\vec{k}_a$ and $\vec{k}_b$:

$$\frac{a}{\pi}\frac{b}{\pi}\int dk_a^x\, dk_a^y\, \exp[-(a+b)(k_a^y{}^2)]\exp[-a(k_a^x)^2 - b(k_a^x - (1-z)p_T)^2] = \frac{1}{\pi}\frac{ab}{a+b}\exp\left\{-\frac{ab}{a+b}[(1-z)p_T]^2\right\}. \tag{A4}$$

Here we have also neglected the weaker dependence of $d\sigma/d\hat{t}$ on $\vec{k}_a$ and $\vec{k}_b$. We define

$$\frac{ab}{a+b} = \frac{1}{2\langle k^2\rangle} . \tag{A5}$$

The maximum point of the integrand in (A4) occurs at $k_a^x = k_b^x = [(1-z)/2]p_T$. We thus see that for z near one, the approximations mentioned above are consistent. This will be typical for all three cases, and means that for nearly symmetric pairs the complications due to the transverse fluctuations are minimal. At the maximum point

$$x_a = x_b = \sqrt{z}\,\frac{2p_T}{\sqrt{s}} \tag{A6}$$

and the invariants of the $ab \to CD$ subprocess have the values appropriate to 90° scattering:

$$|\hat{t}| = |\hat{u}| = \tfrac{1}{2}\hat{s} = 2z\,p_T{}^2 . \tag{A7}$$

We obtain [including a $(1+z)/s\sqrt{z}$ Jacobian factor]

$$E_C E_D \frac{d\sigma}{d^3p_C d^3p_D} = \frac{1}{\pi}\frac{1+z}{2\sqrt{z}}\frac{1}{2\pi\langle k^2\rangle} x_a G_{a/A}(x_a) x_b G_{b/B} \exp\left[-\frac{(1-z)^2 p_T{}^2}{2\langle k^2\rangle}\right]\frac{d\sigma}{d\hat{t}}\bigg|^{ab\to CD}_{\hat{s}=4z p_T{}^2,\ \hat{t}=-2z p_T{}^2} . \tag{A8}$$

From this formula, using the parametrizations of the structure functions and the cross section given in formulas (2.6)–(2.8) we immediately get the expressions (2.10).

In the second case, illustrated in Fig. 2(b), with one final fragmentation, expression (2.7) takes the form

$$\begin{aligned}
E_C E_D \frac{d\sigma}{d^3p_C d^3p_D} = \frac{s}{2\pi}\int dw_d\, dx_a\, dx_b\, d^2k_a\, d^2k_b\, d^2k_d\, x_a G_{a/A}(x_a, \vec{k}_a) x_b G_{b/B}(x_b, \vec{k}_b)\\
\times \frac{D_{D/d}(w_d, \vec{k}_d)}{w_d{}^2}\frac{d\sigma^{ab\to Cd}}{d\hat{t}}\,\delta^4(p_a + p_b - p_C - p_d) .
\end{aligned} \tag{A9}$$

The momenta configuration is as in (A2), except that we have now a new relation between p_D and p_d; including the transverse fluctuation $\vec{k}_d$ we have

$$\vec{p}_d = \frac{\vec{p}_D}{w_d} + \vec{k}_d . \tag{A10}$$

The transverse fluctuations in the fragmentation functions are often taken to be Gaussian, as defined in formula (2.3). To a good approximation the components of k_d in the z and x directions may be neglected and $k_d^y = k_d \sin\phi$ where ϕ is the azimuthal angle of $\vec{k}_d$ about the primary direction $\vec{p}_d$. The three-momenta part of the δ^4 function then yields

$$\begin{aligned}
&x_a = x_b ,\\
&k_a^y + k_b^y - k_d^y = 0,\\
&k_a^x + k_b^x - p_T(1 - z/w_d) = 0 .
\end{aligned} \tag{A11}$$

For strong k_a k_b and k_d damping we obtain the transverse integral

$$\frac{a}{\pi}\frac{b}{\pi}\frac{d}{\pi}\int dk_a^y\, dk_d^y\, e^{-a(k_a^y)^2} e^{-d(k_d^y)^2} e^{-b(k_a^y-k_d^y)^2} \int dk_a^x\, dk_d^x\, e^{-d(k_d^x)^2} e^{-a(k_a^x)^2} e^{-b[k_a^x-p_T(1-z/w_d)]^2} \tag{A12}$$

which reduces to

$$\sim \frac{1}{2\pi\langle k^2\rangle}\left(\frac{2\langle k^2\rangle}{2\langle k^2\rangle+\langle l^2\rangle}\right)^{1/2} \exp\left[-\frac{(1-z/w_d)^2 p_T^{\,2}}{2\langle k^2\rangle}\right], \tag{A13}$$

where we have defined $\langle l^2\rangle \equiv 1/d$ to specify the average fragmentation fluctuation. It is clear that $z \approx w_d$ is preferred. The energy-conservation δ function then can be approximated by

$$(x_a+x_b)\tfrac{1}{2}\sqrt{s} = p_T(1+z/w_d) \tag{A14}$$

or

$$x_a = x_b = (2p_T/\sqrt{s})\tfrac{1}{2}(1+z/w_d)\,. \tag{A15}$$

The $\hat{s}$ of the subprocess is best constructed from the final momenta:

$$\hat{s} = 4p_T^2 z/w_d\,. \tag{A16}$$

Inserting the explicit parametrizations for $G_{a/A}$, $G_{b/B}$, $d\sigma/d\hat{t}$, and $G_{D/d}$ from formulas (2.6)–(2.8), we get

$$E_C E_D \frac{d\sigma}{d^3p_C\, d^3p_D} = \frac{1}{\pi}\frac{1}{2\langle k^2\rangle}\left(\frac{2\langle k^2\rangle}{2\langle k^2\rangle+\langle l^2\rangle}\right)^{1/2} \Lambda_{a/A}\Lambda_{b/B}\, \mathfrak{D}_{90^\circ}^{ab\to cd}\, \frac{(1-x_T)^{g_{a/A}+g_{b/B}}}{(2p_T)^{2N}}\, I(z,p_T)\,, \tag{A17}$$

where

$$I(z,p_T) = d_{D/d}\int_{p_D/(\sqrt{s}-p_C)}^1 \frac{dw_d}{w_d^{\,2}}\left(\frac{1-x_T(1+z/w_d)^2}{(1-x_T)}\right)^{g_{a/A}+g_{b/B}} \frac{w_d^{\,N+g_{D/d}-1}}{z^N}\left(\frac{1}{w_d}-1\right)^{g_{D/d}}$$
$$\times \exp\left[-\frac{(1-z/w_d)^2 p_T^{\,2}}{2\langle k^2\rangle}\right]. \tag{A18}$$

We can, of course, integrate this expression numerically. In order to obtain a useful analytic approximation, we change variables and obtain

$$I(z,p_T) = \frac{d_{D/d}}{z^2}\,\frac{(2\langle k^2\rangle)^{1/2}}{p_T}\int_{-(1-z)p_T/(2\langle k^2\rangle)^{1/2}}^1 d\alpha\, e^{-\alpha^2}\left(1-\frac{x_T}{2(1-x_T)}\,\frac{\alpha(2\langle k^2\rangle)^{1/2}}{p_T}\right)^{g_{a/A}+g_{b/B}}$$
$$\times \frac{1}{\left(\alpha\dfrac{(2\langle k^2\rangle)^{1/2}}{p_T}+1\right)^{N+g_{D/d}-1}}\left(1-z+\alpha\,\frac{(2\langle k^2\rangle)^{1/2}}{p_T}\right)^{g_{D/d}}. \tag{A19}$$

For $z \neq 1$, and p_T reasonably large compared to $2\langle k^2\rangle$, the integral is well approximated by setting $\alpha = 0$ in the factors multiplying the Gaussian and we get

$$I(z,p_T) = \frac{1}{z}\, D_{D/d}(z)\sqrt{\pi}\,\frac{(2\langle k^2\rangle)^{1/2}}{p_T}\,. \tag{A20}$$

For $z = 1$ we have a zero from the D functions as $\alpha^{g_{D/d}}$. A good approximation is obtained by evaluating the factors multiplying $\alpha^{g_{D/d}}\, e^{-\alpha^2}$ at the maximum of that expression. We then get

$$\bar{\alpha} = \left(\frac{g_{D/d}}{2}\right)^{1/2}, \tag{A21}$$

$$I(1,p_T) \sim \bar{I}\, d_{D/d}\left(\frac{2\langle k^2\rangle}{p_T}\right)^{g_{D/d}+1}\int_0^\infty \alpha^{g_{D/d}}\, e^{-\alpha^2}\alpha\,, \tag{A22}$$

where $\bar{I}(x_T, N, g_{D/d}, g_{a/A}+g_{b/B})$ is given by

$$\bar{I} \equiv \frac{\left[1-\frac{x_T}{1-x_T}\,\frac{1}{2}\left(\frac{g_{D/d}}{2}\right)^{1/2}\frac{(2\langle k^2\rangle)^{1/2}}{p_T}\right]^{g_a/A+g_b/B}}{\left[1+\left(\frac{g_{D/d}}{2}\right)^{1/2}\frac{(2\langle k^2\rangle)^{1/2}}{p_T}\right]^{N+g_{D/d}-1}} . \tag{A23}$$

This is a very good approximation for $g_{D/d}=1$, and only somewhat worse for $g_{D/d}=3$. As can be seen from this analytic approximation, $I(z,p_T)$ approaches the asymptotic limit (9.13) from below. Thus, e.g., for $2<p_T<6$ GeV and $20<\sqrt{s}<30$ GeV, we get for $\pi^+\pi^-$ pairs at $z=1$,

$$E_{\pi^-}E_{\pi^+}\frac{d\sigma}{d^3p_{\pi^-}d^3p_{\pi^+}} \simeq \begin{cases} 0.175\,\dfrac{(1-x_T)^8}{p_T^{10}} & \text{GeV}^{-6}\ \text{(asymptotic formula)},\\ 0.0268\,\dfrac{(1-x_T)^{9.1}}{p_T^{9.1}} & \text{GeV}^{-6}\ \text{(parametrization of numerical integration)}. \end{cases} \tag{A24}$$

Finally we must consider the double-fragmentation case, Fig. 2(c). Here we have two fragmentation functions and

$$E_C E_D \frac{d\sigma}{d^3p_C d^3p_D} = \frac{s}{2\pi}\int dw_d\, dw_c\, dx_a\, dx_b\, d^2k_a\, d^2k_b\, d^2k_c\, d^2k_d\, x_a G_{a/A}(x_a,\vec{k}_a)\, x_b G_{b/B}(x_b,\vec{k}_b)$$
$$\times \frac{D_{C/c}(w_c,\vec{k}_c)}{w_c^2}\,\frac{D_{D/d}(w_d,\vec{k}_d)}{w_d^2}\,\delta^4(p_a+p_b-p_c-p_d)\,\frac{d\sigma^{ab\to cd}}{d\hat{t}} . \tag{A25}$$

We have the same momenta definitions as before only with

$$\vec{p}_c=\frac{\vec{p}_C}{w_c}+\vec{k}_c,\quad \vec{p}_d=\frac{\vec{p}_D}{w_d}+\vec{k}_d . \tag{A26}$$

The δ^4 function now yields, for small $|\vec{k}_a|$ and $|\vec{k}_b|$,

$$\begin{aligned} &x_a\tfrac{1}{2}\sqrt{s}-x_b\tfrac{1}{2}\sqrt{s}=0,\\ &\frac{p_T}{w_c}-\frac{zp_T}{w_d}=0,\\ &k_a^y+k_b^y-k_c^y-k_d^y=0,\\ &x_a\tfrac{1}{2}\sqrt{s}+x_b\tfrac{1}{2}\sqrt{s}-\left(\frac{p_T}{w_c}+\frac{zp_T}{w_d}\right)=0, \end{aligned} \tag{A27}$$

with k_a^x, k_b^x, k_c^x and k_d^x unconstrained except to be much less than p_T, because of the Gaussian falloff. We can do the $k_{a,b}^x$ and $k_{c,d}^x$ transverse integrals trivially, leaving k_i^y integrals of the form

$$\left(\frac{c}{\pi}\frac{d}{\pi}\frac{a}{\pi}\frac{b}{\pi}\right)^{1/2}\int dk_a^y\, dk_b^y\, dk_c^y\, e^{-d(k_a^y+k_b^y-k_c^y)^2}e^{-a(k_a^y)^2-b(k_b^y)^2-c(k_c^y)^2}=\frac{1}{\sqrt{\pi}}\,\frac{1}{\left(\frac{1}{a}+\frac{1}{b}+\frac{1}{c}+\frac{1}{d}\right)^{1/2}}\equiv\frac{1}{\sqrt{2\pi}}\,\frac{1}{(\langle k^2\rangle+\langle l^2\rangle)^{1/2}} . \tag{A28}$$

(Note that had we defined k_d and k_c as the transverse momenta of the hadrons relative to their source quarks, rather than of the quarks relative to the hadrons, e.g., $\vec{p}_d=\vec{p}_D/w_d-\vec{k}_d/w_d$; our final formula would be altered.) The w_c integral now yields

$$\int\frac{dw_c}{w_c^2}\,\delta\left(\frac{p_T}{w_c}-\frac{zp_T}{w_d}\right)=\frac{1}{p_T} , \tag{A29}$$

$$x_a=x_b=\frac{2p_T}{\sqrt{s}}\,\frac{z}{w_d} , \tag{A30}$$

with a net $2/s$ Jacobian. The subprocess cross section is evaluated at 90° with $\hat{s}=4p_T^2z^2/w_d^2$. We are

left with the form

$$E_C E_D \frac{d\sigma}{d^3p_C d^3p_D} = \frac{1}{[2\pi(\langle k^2\rangle + \langle l^2\rangle)]^{1/2} p_T} \int_{x_T z}^{z} \frac{dw_d}{w_d^2} \Lambda_{a/A}\Lambda_{b/B} d_{D/d} d_{C/c} \frac{\mathfrak{D}_{90^\circ}^{ab\to cd}}{\left(\frac{4p_T^2 z^2}{w_d^2}\right)^N} (1 - x_T z/w_d)^{g_{a/A}+g_{b/B}} \times \frac{(1-w_d/z)^{g_{C/c}}}{(w_d/z)} \frac{(1-w_d)^{g_{D/d}}}{w_d} \tag{A31}$$

in terms of the parameters defined in (2.6)–(2.8).

For an approximate analytic expression we note that since w_d is constrained to lie between zx_T and z we can make the variable change

$$w_d = z\bar{w}, \quad \bar{w} = 1 - (1-x_T)\beta \ , \tag{A32}$$

and use mean-value techniques to perform the β integration.

We obtain

$$\bar{\beta} = \frac{g_{C/c}}{g_{a/A} + g_{b/B} + g_{C/c}} \quad \text{for } z \neq 1$$

and

$$E_C E_D \frac{d\sigma}{d^3p_C d^3p_D} \underset{z\neq 1}{=} \frac{1}{[2\pi(\langle k^2\rangle + \langle l^2\rangle)]^{1/2} p_T} \Lambda_{a/A}\Lambda_{b/B} d_{D/d} d_{C/c} \times \frac{\mathfrak{D}_{90^\circ}^{ab\to cd}}{(4p_T^2)^N} \frac{(1-x_T)^{g_{a/A}+g_{b/B}+g_{C/c}+1}}{z^2} \frac{\Gamma(g_{a/A}+g_{b/B}+1)\Gamma(g_{C/c}+1)}{\Gamma(g_{a/A}+g_{b/B}+g_{C/c}+2)} \times [1-(1-x_T)\bar{\beta}]^{2N-g_{a/A}-g_{b/B}-4} [1 - z + z(1-x_T)\bar{\beta}]^{g_{D/d}} \ . \tag{A33}$$

Note that for $z \neq 1$ the double-fragmentation scaling law and the single-fragmentation scaling law are the same:

$$\frac{1}{\sqrt{\langle k^2\rangle}\, p_T^{2N+1}} \ .$$

For fixed $\Delta p_T = (1-z)p_T$, $z \to 1$ as $p_T \to \infty$ and a different approximate analytic form applies

$$E_C E_D \frac{d\sigma}{d^3p_C d^3p_D} \overset{z\to 1}{=} \frac{1}{[2\pi(\langle k^2\rangle + \langle l^2\rangle)]^{1/2}} \frac{1}{p_T} \Lambda_{a/A}\Lambda_{b/B} d_{D/d} d_{C/c} \frac{\mathfrak{D}_{90^\circ}^{ab\to cd}}{(4p_T^2)^N} (1-x_T)^{g_{a/A}+g_{b/B}+g_{C/c}+g_{D/d}} \times \frac{\Gamma(g_{a/A}+g_{b/B}+1)\Gamma(g_{C/c}+g_{D/d}+1)}{\Gamma(g_{a/A}+g_{b/B}+g_{C/c}+g_{D/d}+2)} [1-(1-x_T)\hat{\beta}]^{(2N-4-g_{a/A}-g_{b/B})} , \tag{A34}$$

with

$$\hat{\beta} = \frac{g_{C/c}+g_{D/d}}{g_{a/A}+g_{b/B}+g_{C/c}+g_{D/d}} \ .$$

Corrections are of order $\Delta p_T / p_T$. Note that in both double-fragmentation situations the symmetric-pair cross section scales with one more power than the single-particle cross section based on the same subprocess. For later use we define the function

$$\bar{J}(x_T) = \frac{[1-(1-x_T)\hat{\beta}]^{2N-4-g_{a/A}-g_{b/B}}}{[2(\langle k^2\rangle + \langle l^2\rangle)]^{1/2}} (1-x_T)^{g_{a/A}+g_{b/B}+g_{C/c}+g_{D/d}} \ . \tag{A35}$$

The approximation (A34) to the true integral is good to 20% for $x_T > 0.6$.

[1]R. Blankenbecler, S. Brodsky, and J. F. Gunion, Phys. Rev. D 18, 900 (1978); M. K. Chase and W. J. Stirling, Nucl. Phys. B133, 157 (1978).
[2]R. D. Field, in *Proceedings of the XIX International Conference on High Energy Physics, Tokyo, 1978,* edited by S. Homma, M. Kawaguchi, and H. Migazawa (Phys. Soc. of Japan, Tokyo, 1979), and references therein.
[3]W. E. Caswell, R. R. Horgan, and S. J. Brodsky, Phys. Rev. D 18, 2415 (1978).
[4]R. Baier, J. Engels, and B. Peterson, Bielefeld Report No. BI-TP 79/10, 1979 (unpublished); Z. Phys. C (to be published).
[5]D. Jones and J. F. Gunion, Phys. Rev. D 19, 867 (1979).
[6]H. Jöstlein *et al.*, Phys. Rev. Lett. 42, 146 (1979); Phys. Rev. D 20, 53 (1979).
[7]ISR collaboration, M. G. Albrow *et al.*, Nucl. Phys. B145, 305 (1978).
[8]C. Bromberg *et al.*, Phys. Rev. Lett. 43, 561 (1979).
[9]H. J. Frisch *et al.*, Phys. Rev. Lett. 44, 511 (1980).
[10]R. Field, private communication.
[11]The $z \neq 1$ cases are discussed in the Appendix and the results of Sec. III.
[12]D. A. Finley *et al.*, Phys. Rev. Lett. 42, 1028 (1979); 42, 1037 (1979).
[13]H. Bøggild, in Proceedings of the XIV Rencontre de Moriond, 1979, edited by Trân Thanh Vân (unpublished).
[14]M. J. Tannenbaum, in Proceedings of the XIV Rencontre de Moriond, 1979, edited by J. Trân Thanh Vân (unpublished).
[15]C. Kourkoumelis *et al.*, Phys. Lett. 86B, 391 (1979).
[16]J. Gunion and B. Petersson, work in progress.
[17]See the talk by M. Jacob at EPS meeting, Geneva, Switzerland, 1979 [Report No. CERN-TH 2700 (unpublished)].